NACA RM A57E24

NACA

RESEARCH MEMORANDUM

INVESTIGATION OF AXIALLY SYMMETRIC FLOW OVER STEPS AT TRANSONIC SPEEDS WITH COMPARISONS OF ESTIMATED AND EXPERIMENTAL DRAG RESULTS

By George H. Holdaway and Minor R. Wallace, Jr.

Ames Aeronautical Laboratory
Moffett Field, Calif.

NATIONAL ADVISORY COMMITTEE
FOR AERONAUTICS
WASHINGTON

July 22, 1957
Declassified September 1, 1959

NATIONAL ADVISORY COMMITTEE FOR AERONAUTICS

RESEARCH MEMORANDUM

INVESTIGATION OF AXIALLY SYMMETRIC FLOW OVER STEPS AT TRANSONIC SPEEDS WITH COMPARISONS OF ESTIMATED AND EXPERIMENTAL DRAG RESULTS

By George H. Holdaway and Minor R. Wallace, Jr.

SUMMARY

This investigation was directed primarily toward the problem of predicting the experimental wave drag for configurations which have discontinuities in area distribution and thus infinite theoretical wave drag. Rings of three different heights were tested at transonic speeds on a body of revolution to form forward- and rearward-facing steps. The basic body was a fineness-ratio-12.5 Sears-Haack body. The rings were also tested with 10° fillets to remove the step in the area distribution. Adding a 10° fillet rearward of the ring caused almost no reduction in experimental total drag, whereas a 10° fillet forward of the ring caused reductions up to 60 percent.

As expected, the agreement between the experimental and computed wave drags of the ring-body combinations without fillets was very poor. When fillet areas, to remove the step in the area curves, were assumed for the computations, the agreement was improved; however, for the larger rings, drag differences as large as 200 percent were still obtained.

The total drag of the ring models was estimated with good accuracy by simply adding to the experimental basic-body drag an increment computed from the measured pressures on the faces of the rings. These face pressures were also used to study the analogous problem (steps in the area distribution curve) of ducted bodies operating at reduced mass-flow ratios. Comparison of estimated results based on the ring-face pressures with experimental results indicated that reasonable estimates of the total-drag increases with reduced mass-flow ratios could be made.

INTRODUCTION

A procedure for the computation of the zero-lift wave drag of airplanes based on the theory of reference 1 has been developed (ref. 2)

which is practical and accurate, provided certain limits of the theory are not exceeded. These limits are discussed in reference 3 which also calls attention to local lift effects which should be considered for asymmetrical configurations at supersonic speeds. An important limitation of the theory, and thus the computing procedure, is that in general there must be no discontinuity in any area distribution or the derivative of the area distribution intercepted on the airplane by any set of cutting planes; that is, all component parts of the airplane and the total airplane are slender with smooth cross-sectional area distributions. (Discontinuities in the derivative of other than the normal area distribution are admissible in the theory if the discontinuities are integrable, that is, logrithmic singularities.) However, it was noted in references 2 and 4 that with slight nonintegrable discontinuities in the derivative of the area distributions, reasonably accurate wave-drag coefficients were computed if the harmonic analysis was limited to about 25 terms. The calculated values were for area distributions inherently smoothed by the harmonic analysis, and it was suggested in reference 2 that small discontinuities might actually be smoothed by the boundary-layer effects. On the other hand, for configurations with discontinuities in area distribution (e.g., produced by an engine duct with a mass-flow ratio other than 1.0), the computed "smoothed" area distribution and the wave drag varied markedly with the number of harmonics used to represent the area distribution. As brought out in reference 2, this is to be expected because if an infinite number of harmonics were used to represent the exact area distribution, an infinite drag would be predicted when there is a step in the area curve.

Investigations of the flow over two-dimensional steps such as those reported in references 5, 6, and 7 indicated that a wedge of separated flow generally occurred ahead of the step. In each case it was observed that the separated flow region was not completely stationary, because there was some circulation or mixing within the pseudo dead-air region. However, a possible approach to obtain finite wave-drag computations in reasonable agreement with experimentation would be to assume the "wedge" to be dead air and add its area distribution to that of the existing configuration. This would tend to tie in with the concept that potential theory for a body would be more exact, relative to experiment, if the displacement thickness of the boundary layer were added to the body radii. A study of pressure ratios and schlieren pictures of reference 7 indicated that for two-dimensional turbulent flow, the wedge angle for a forward- or rearward-facing step was approximately 10° at a Mach number of 1.3. This separation angle increased slightly with increasing Mach number to about 13° and 17° at $M = 3.00$ for a forward- and rearward-facing step, respectively. The previously mentioned references on separated flow over steps did not include transonic data.

The present investigation was undertaken to gain some insight into the problem of predicting the experimental wave drag of a configuration which has a discontinuity in its area distribution and to provide some

transonic data for separated flow over steps. The harmonic-analysis method of reference 2 was used to predict the wave drag, and the solutions were limited to 25 harmonics which have been adequate and most commonly used in previous applications of the method. The configuration selected for study was a body of revolution with a ring located near the body maximum diameter to produce forward- and rearward-facing steps. Three ring sizes were chosen to provide a variation in the magnitude of the step discontinuity. In addition, fillets with a slope of 10° were provided to fair in the forward and/or the rearward edges of the rings for some of the tests. The smallest ring was selected to simulate roughly a possible change in area distribution due to a change in mass-flow ratio for a scoop-type duct similar to that discussed in reference 2.

SYMBOLS

C_{D_o}	zero-lift drag coefficient, $\frac{\text{drag at zero lift}}{qS_b}$
ΔC_{D_o}	experimental drag-rise coefficient above subsonic level at $M = 0.90$ or theoretical wave-drag coefficient, both at zero lift
C_p	pressure coefficient, $\frac{p_l - p}{q}$
h	step height
$L(x)$	projection of resultant force on oblique section
l	fuselage length
M	free-stream Mach number
N	number of terms or harmonics used in the Fourier sine series
p_l	body-surface local pressure
p	free-stream static pressure
q	free-stream dynamic pressure
R	Reynolds number
r_o	body radius at maximum diameter
S	projection of S_s on plane perpendicular to the x axis
S_b	maximum cross-sectional area of basic Sears-Haack body

S_f face area of ring

S_s area formed by cutting configuration with parallel planes tangent to the Mach cone

x coordinate along the longitudinal axis of the body

$\int_0^x \frac{\beta L(x)}{2q} dx$ equivalent area distribution of the oblique force term, reference 3

β $\sqrt{M^2 - 1}$

MODELS AND TESTS

The basic body and three rings, each 6 inches in length but of different step heights, are defined by an equation and a geometric sketch in figure 1(a). The rings had step heights corresponding to increases in maximum body diameter of 11.1, 22.2, and 33.3 percent, and will be referred to hereafter as rings A, B, and C, respectively. The basic body was a Sears-Haack body (a minimum-wave-drag body for prescribed volume and length), and had a closed-body fineness ratio of 12.5 and a maximum radius of 4.5 inches. The rings were centrally located near the maximum diameter of the body. For some tests, 10° fillets which eliminated the steps in the area distributions as shown in figure 1(b) were added ahead of and behind the rings. A photograph of ring A and the basic body mounted on the sting in the test section of the Ames 14-foot transonic wind tunnel is shown in figure 2.

The Ames 14-foot transonic wind tunnel is a closed-return type with perforated walls in the test section. Sectional sketches of the high-speed regions of this transonic test facility are presented in figure 3. The flexible walls ahead of the test section are controlled to produce the convergent-divergent nozzle required to generate supersonic Mach numbers up to 1.20. This tunnel is similar to the smaller Ames 2- by 2-foot transonic wind tunnel which is described in detail in reference 8. One exception, however, is that the 14-foot tunnel is not of the variable-density type, but operates at atmospheric pressures. Models are mounted on a sting and the forces are measured as electrical outputs from a strain-gage balance located within the model.

The test data included schlieren pictures and force and pressure measurements taken at zero angle of attack. The location of the pressure orifices on the bodies is shown in figure 4. Three radial positions of pressure orifices were used on the body to provide more accurate pressure distributions. Note that more complete pressure measurements were taken

with ring A than with rings B and C. The Reynolds number per foot for these tests was about 4,500,000 throughout the test Mach number range of 0.80 to 1.20 as shown in figure 5. The Reynolds number based on the distance from the body nose to the forward face of the step was almost 20,000,000 for the tests. Turbulent flow in the boundary layer was insured by fixing transition with size 60 grit Carborundum distributed over the forward inch of the body nose as shown in figure 2.

RESULTS AND DISCUSSION

The results will be presented and discussed in two sections. The first part will be concerned with the experimental drag coefficients and the estimation of the wave drag, and the second part will deal primarily with the pressure data and a procedure for the estimation of the total drag. In each case the data are for zero angle of attack and zero lift.

Drag Coefficients and the Estimation of Wave Drag

The experimental drag coefficients for the basic body with various rings and fillets are presented in figure 6. Figure 6(a) contains the data for the smallest ring (ring A) and illustrates the effect of adding either the forward 10° fillet, the rearward 10° fillet, or both fillets. An interesting observation that can be made from this figure is that at transonic speeds the rearward fillet caused almost no reduction in the drag coefficients, whereas the forward fillet caused a substantial reduction, approximately equal to that with both fillets (15 to 40 percent). Similar results were obtained with the larger rings; however, for these models the reductions in drag coefficients due to the forward fillet were of the order of 20 to 60 percent (figs. 6(a) and 6(b)). The rearward fillets were partially effective in reducing the drag coefficients at the lowest and highest test speeds.

Because of the decrease in drag coefficient with increase in Mach number from 0.80 to 0.90 for the body with ring C and the slight drag-coefficient differences between the two Mach numbers for the other two rings, $M = 0.90$ was selected as the reference for computing the drag-rise coefficients for the ring-body models without fillets. Further, the turbulent friction-drag coefficient variation with Mach number is slight for these tests (0.002, based on the charts of ref. 9) and was therefore neglected. For these two conditions, the experimental drag-rise coefficients shown in figure 7 for the ring-body models are considered as representing the theoretical wave-drag coefficients. It is obvious that the computed results greatly overestimate the experimental drag-rise coefficients except for the smallest step. For these calculations the wave-drag coefficients were computed from area curves for Sears-Haack bodies to closure

and were corrected by subtracting the estimated contribution of the cut-off portion (ΔC_{D_0} = 0.0118 based on a theoretical pressure distribution for M = 1.20). The flagged symbols indicate the computed wave-drag coefficients for the rings with two assumed 10° dead-air fillets.

As mentioned previously, the 10° fillets were assumed in order to simulate the boundary of the retarded air ahead of and behind the rings, and thus obtain a configuration which would have finite theoretical wave drag. As shown in figure 7, the computed results for ring A were only slightly affected by the addition of assumed fillets to the area curves analyzed. For rings B and C the magnitude and trends of the experimental data at supersonic speeds were more nearly predicted by the addition of the assumed fillets; however, the results indicate that the assumption of the 10° fillets to represent the boundary of the retarded-flow regions about the ring-body models without fillets is generally a poor one at transonic speeds. The schlieren pictures also indicate that the assumption of the 10° angle does not in general represent the boundary of the air flow about the rings without fillets. Nevertheless, some insight as to the boundary of the flow at transonic speeds over steps is provided by the representative schlieren pictures presented in figure 8 for ring C with and without fillets. Similar schlieren results were obtained for rings A, B, and C, but the separation was more easily seen for the larger ring C. It is evident from figure 8 that the mixing region rearward of the ring at the higher subsonic speeds extends almost straight back from approximately the top of the rearward-facing step whether there is a fillet or not. This mixing region at the rear of the rings was only slightly thinned at M = 1.00 and thus at this Mach number a more logical approximate representation of the flow over the rearward-facing step would be a constant area distribution for the rear half of the body equal to the maximum frontal area of the ring and body. This assumption is approximate but more exact measurements from the schlieren pictures did not seem to be justified due to the evident mixing of the air. Based on the assumption of a 10° forward fillet and a constant area for the rear half of the body the revised wave-drag coefficients for M = 1.00 were as follows:

Ring	Computed		Experiment
	10° fillets	Revised	
A	0.2107	0.0847	0.1329
B	0.5919	0.2268	0.2573
C	0.8177	0.3458	0.3671

It is evident that the revised computations agree much better with experiment, particularly for rings B and C. Such agreement is fortuitous because it is well known that the theory does not apply at M = 1.00 and therefore agreement with experiment is not to be expected; however, these comparisons are intended to indicate that equivalent fairing of

discontinuities by viscous effects may account for some of the fortuitous agreement between predicted and experimental drag coefficients for configurations with discontinuities in area distribution. As the Mach number increases above 1.00 the mixing regions apparently approach the assumed fillet shapes, as indicated (more clearly for the rearward-facing step) in figure 8. The bottom picture in figure 8(c) indicates that at $M = 1.20$ the boundary of the air flow ahead of the forward-facing step is similar to that anticipated on the basis of prior two-dimensional results. The air flow at $M = 1.20$ seems to be attached to the rearward fillet and separated in front of the step, with the boundary of the retarded-air fillet extending from the forward shock wave to the top of the step with a form approximating the rearward fillet. Thus, at $M = 1.20$ the assumption of 10° fillets appears at first to be a reasonable approximation to the boundary of the retarded-air region. However, a more detailed study reveals that this is not the case. Some mixing of the air within the retarded-air region appears to be likely from the schlieren pictures, and the total drag data of figure 6 shows a marked change in drag of the ring-body model as a result of adding the forward fillet.

Even though the prior discussion indicates the inadequacy of the assumed 10° fillets in representing the boundary of the flow about the ring-body models without fillets, it is interesting to note that some similarity does exist between the experimental drag-rise coefficients of the models with and without fillets. This is illustrated in figure 9 which presents the experimental drag-rise coefficients above $M = 0.90$. On the basis of these data alone one might have concluded that the assumption of 10° fillets was a reasonable one.

Considering again the computed wave-drag coefficients for the ringed bodies, it is of interest to note the actual shapes represented by the computations limited to 25 harmonics. Figures 10(a), 10(b), and 10(c) present such shapes which are identified in the figures as check solutions. It is quite evident, particularly at $M = 1.00$ (fig. 10(a)), that the solutions are for wavy bodies which tend to fair the steps in the area curves due to the rings but fit the original area curves very poorly. The best representations are for ring A and the higher Mach numbers where the computations tended to approach the experimental values. The waviness which extends over the entire length of the bodies partially accounts for the extreme wave-drag coefficients computed for rings B and C (presented earlier in fig. 7) and is not characteristic of the viscous effects. It should be noted that a sizable difference between computations and experimental data continued to exist after the waviness was reduced by the addition of assumed fillets.

The effect of adding fillets was beneficial in improving the agreement between the given area curves and the check solutions as shown by the solutions for $M = 1.20$ presented in figure 11. With the agreement shown in figure 11, one would expect very slight differences between computed and measured drag-rise coefficients for the model with both fillets. This

was not the case for the larger ring models for experimental drag-rise coefficients above $M = 0.90$ as may be seen from the following table for the ring models with forward and rearward fillets ($M = 1.20$).

Ring	Computed wave-drag coefficients	Experimental drag-rise coefficients	
		Above $M = 0.9$	Above $M = 0.8$
A	0.1602	0.1655	0.1751
B	0.3865	0.2499	0.3105
C	0.5380	0.2845	0.4412

The data of figures 6 and 8(b) clearly indicate for the ring-body models with fillets that if $M = 0.8$ is used as the subsonic drag level a more accurate appraisal of the drag-rise coefficients could be made. As shown in the preceding table, for this reference Mach number, the agreement between computed and experimental drag-rise coefficients is more nearly of the order to be expected from an examination of the given area curves and check solutions shown in figure 11.

The computed wave-drag coefficients so far discussed neglected the oblique forces considered in the more complete wave-drag equation presented in reference 3 (i.e., $\beta L(x)/2q$). Neglecting the oblique force or "lift" term at Mach number 1.00 is fully justified ($\beta = 0$); however, at supersonic speeds this factor is zero only for symmetrical, smooth, high-fineness-ratio bodies. A plot of the magnitude of the "lift" term for ring A at $M = 1.20$ in terms of equivalent area distribution is shown in figure 12. For the combined area-distribution curve of figure 12 corrected for the cut-off body the computed drag coefficient is 0.1880. Since this value for the smallest ring is greater than the previous computation (which was in turn greater than the experimental results), it is evident that the failure to get agreement with experimentation for all the rings is not due to ignoring the pressure term. The oblique forces were computed from pressure measurements which will be discussed next.

Pressure Coefficients and the Estimation of Total Drag

An example of the experimental pressure-coefficient distributions for three radial positions for each ring model is shown in figure 13 for $M = 1.00$. The pressure coefficients for the basic body without a ring are shown by the dashed curve and were obtained from reference 10. From data similar to figure 13 it was evident for ring A that the

peak-pressure coefficients, as defined in the accompanying sketch, were not measured by the pressure orifices in the original model, particularly at the rear of the step; therefore, additional pressure orifices were added to this model as discussed previously in connection with figure 4. These additional data points are shown in figure 14 which also presents the faired data curves for each ring model at various Mach numbers. The peak pressures for ring C were measured, but generally those for ring B were only approximated.

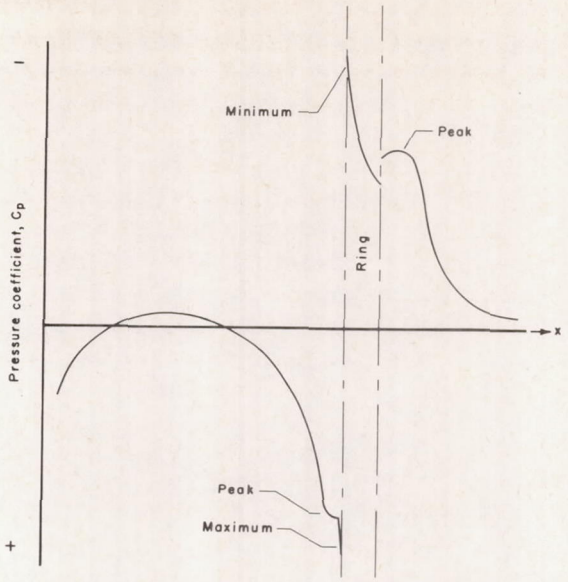

It is of interest to note that the pressures near the forward face of the rings are more positive than the pressures at the rear of the rings are negative, even though the negative pressures of the basic body tend to make the pressures near the rear of the step numerically greater. This indicates that the largest contribution to the drag of the ring-body models comes from the forward-facing step and this fact partially explains the greater reduction in drag obtained with the forward fillet in comparison with the rearward fillet; although, the major portion of the drag reduction is probably due to the change in pressures resulting from the addition of the forward fillet.

Peak-pressure coefficients for the forward-facing steps have been plotted in figure 15 along with the two-dimensional supersonic results of reference 7; the coefficients have been converted to a notation similar to that used in reference 7. The data of reference 7 indicate that the pressure coefficients for the separation point tend to merge at the lower supersonic speeds with the peak-pressure coefficients and the trend of this two-dimensional data merges with the trend of the axially symmetric three-dimensional data of this report. It is also of interest to note that there is a consistent increase in this peak-pressure coefficient with increase in the height of the step at each Mach number with greater increases occurring at the higher Mach numbers.

Realizing that the pressures on the flat top of the rings would not contribute to the drag of the models and that the pressures on the slightly curving body near the rings would contribute very little to the drag, it was concluded that the pressures on the forward and rearward faces of the steps would be the primary variables affecting the total drag of the models. Figure 16 contains faired curves of the pressure-coefficient variation with Mach number for the forward and rearward faces of ring A, and approximate face pressure coefficients for rings B and C

obtained from pressure orifices located on the body near the ring faces. Rings A and B have almost identical pressures at their forward face and the pressures at their rearward face follow consistent and similar trends which should be representative of rings of similar or smaller sizes similarly mounted in pressure fields of almost zero gradient. The variation with Mach number of the face pressures for ring C is roughly similar to that of the other rings, but the pressures on the forward face are larger and the pressures on the rearward face are more erratic. The dip in the pressure coefficients for the rearward face of all the rings at subsonic speeds is probably due to a shock wave moving aft of the step as indicated at $M = 0.9$ in figure 8(a). This is undoubtedly the source of the dip in the drag coefficient of ring model C at this subsonic Mach number (fig. 6(b), ring alone data).

The pressure coefficients of figure 16 were used to compute the total drag of the models with the rings. This was done by simply adding to the experimental drag coefficients of the Sears-Haack body, obtained from reference 10, an increment equal to the difference in the forward- and rearward-face pressure coefficients multiplied by the ratio of the face area of the rings to the maximum cross-sectional area of the basic Sears-Haack body, that is,

$$\delta C_{D_o} = \frac{S_f}{S_b}\left(C_{p_{\text{forward face}}} - C_{p_{\text{rearward face}}}\right)$$

The results of such approximate calculations are shown in figure 17 to be in agreement with the experimental results within about 10 percent or less. These empirical estimates could not have been made prior to this investigation because of the lack of transonic data. Thus, although reasonable estimates at transonic speeds of the wave drag of rings B and C could not generally be made by harmonic analysis, fairly good estimates were made from the face pressures. If the body near the steps had a large amount of curvature in the streamwise direction, the entire pressure distribution in the region of the steps would have to be considered, and should have been considered in this case had greater accuracy been desired.

The pressure data from these tests of bodies with rings were used to study the analogous problem (steps in the area-distribution curve) of ducted bodies operating at various reduced mass-flow ratios. Estimates of the increase in zero-lift drag coefficients with reduced mass-flow ratio are illustrated in figure 18 for two experimental investigations of scoop-type ducts reported in references 2 and 11. The forward- and rearward-face pressures for ring A were used to compute the estimated change in total drag with changes in mass-flow ratio in the same manner as for the preceding estimates of total drag for the ring models. The face pressures of ring A were used because the equivalent area steps due to change in mass-flow ratios (in percentage of the maximum cross-sectional area of the bodies) were less than that of ring A. The possible slight

variation of drag inside the ducts with the differences in mass-flow ratios was neglected. The agreement between the experimental and estimated results is fair and is best at subsonic and supersonic Mach numbers.

SUMMARY OF RESULTS

The primary results of this transonic investigation of bodies at zero lift with forward- and rearward-facing steps formed by a ring around the central region of the body may be summarized as follows:

1. Adding a 10° fillet at the rear of the ring caused almost no reduction in total drag, whereas a 10° fillet forward of the ring caused reductions up to 60 percent.

2. The experimental drag-rise coefficients of the models with rings were altered by the addition of fillets to a much lesser degree than were the total-drag coefficients.

3. The assumption of fillet areas to remove the steps in the area curves generally improved the comparison between experimental and computed wave drags for the ring-body combinations; although, even with this assumption, the computed values for the larger rings were about 200 percent greater than the experimental values.

4. Schlieren pictures indicated that the boundary of the separated region near the steps resembled 10° fillets at $M = 1.20$, but at Mach numbers near 1.00 the "separated" mixing region extended almost straight back from the rearward edge of the ring.

5. Adding the oblique-force term to the wave-drag analysis of the area curve for $M = 1.20$ for the model with the smallest ring resulted in poorer agreement of computed wave-drag coefficients with experimental drag-rise coefficients.

6. The total drag of the ring models was calculated with good accuracy by simply adding to the experimental basic-body drag an increment computed from the measured pressures on the step faces of the rings.

7. A fair estimate of the increase in drag with decrease in mass-flow ratio for two ducted configurations was obtained by utilizing the face pressures measured on the ring models.

Ames Aeronautical Laboratory
National Advisory Committee for Aeronautics
Moffett Field, Calif., May 24, 1957

REFERENCES

1. Jones, Robert T.: Theory of Wing-Body Drag at Supersonic Speeds. NACA RM A53H18a, 1953.

2. Holdaway, George H., and Mersman, William A.: Application of Tchebichef Form of Harmonic Analysis to the Calculation of Zero-Lift Wave Drag of Wing-Body-Tail Combinations. NACA RM A55J28, 1956.

3. Lomax, Harvard: The Wave Drag of Arbitrary Configurations in Linearized Flow as Determined by Areas and Forces in Oblique Planes. NACA RM A55A18, 1955.

4. Nelson, R. L., and Welsh, Clement J.: Some Examples of the Applications of the Transonic and Supersonic Area Rules to the Prediction of Wave Drag. NACA RM L56D11, 1957.

5. Abbott, Ira H.: Some Factors Contributing to Scale Effect at Supersonic Speeds. Fourth Meeting of AGARD Wind Tunnel and Model Testing Panel, London, Sept. 3-11, 1953.

6. Bogdonoff, S. M., and Kepler, C. E.: Separation of a Supersonic Turbulent Boundary Layer. Jour. Aero. Sci., vol. 22, no. 6, June 1955, pp. 414-424, 430.

7. Chapman, Dean R., Kuehn, Donald M., and Larson, Howard K.: Investigation of Separated Flows in Supersonic and Subsonic Streams With Emphasis on the Effect of Transition. NACA TN 3869, 1957.

8. Spiegel, Joseph M., and Lawrence, Leslie F.: A Description of the Ames 2- by 2-Foot Transonic Wind Tunnel and Preliminary Evaluation of Wall Interference. NACA RM A55I21, 1956.

9. Lee, Dorothy B., and Faget, Maxime A.: Charts Adapted from Van Driest's Turbulent Flat-Plate Theory for Determining Values of Turbulent Aerodynamic Friction and Heat-Transfer Coefficients. NACA TN 3811, 1956.

10. McDevitt, John B., and Taylor, Robert A.: An Investigation of Wing-Body Interference Effects at Transonic Speeds for Several Swept-Wing and Body Combinations. NACA RM A57A02, 1957.

11. Merlet, Charles F.: Pressure Recovery and Drag Characteristics of a Forward Located Circular Scoop Inlet as Determined From Flight Tests for Mach Numbers From 0.8 to 1.6. NACA RM L54B23, 1954.

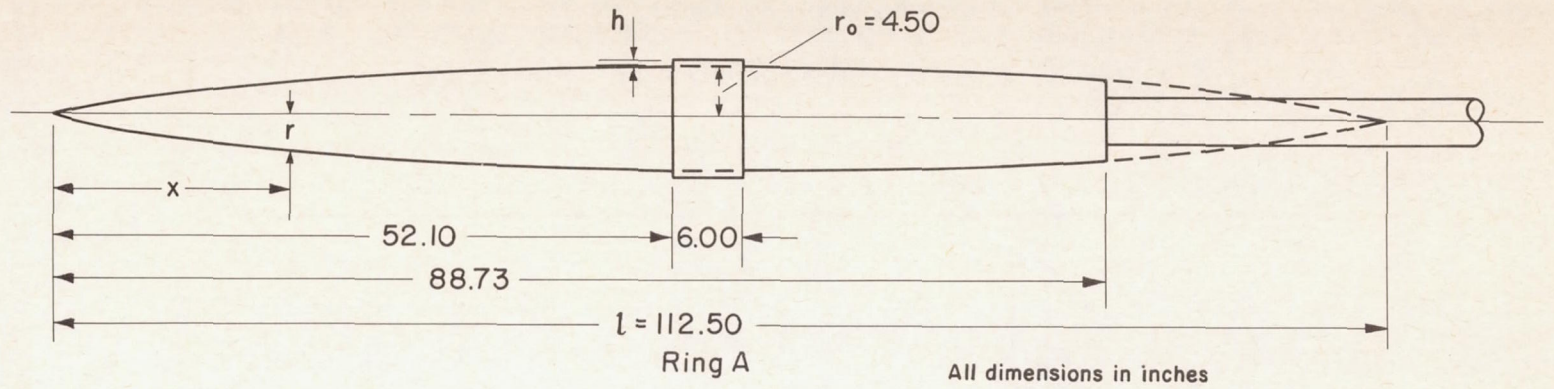

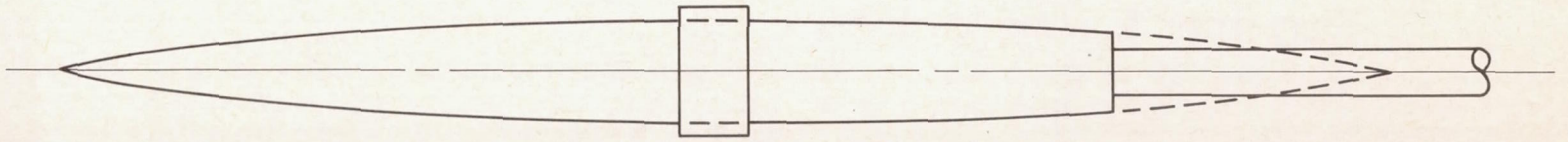

Equation of body radii

$$\frac{r}{r_o} = \left[1-\left(1-\frac{2x}{l}\right)^2\right]^{3/4}$$

Model	h
Ring A	0.50
Ring B	1.00
Ring C	1.50

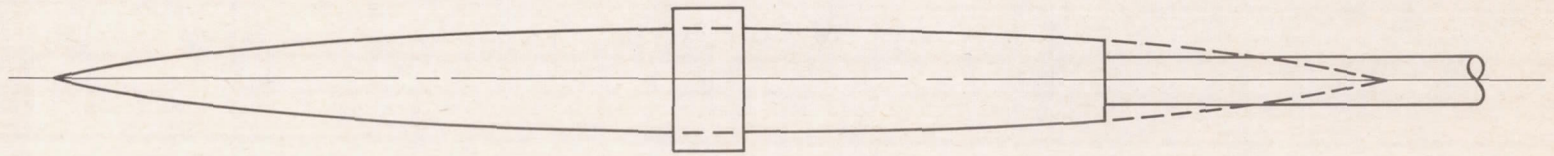

(a) Geometric sketches.

Figure 1.- Ring-body models.

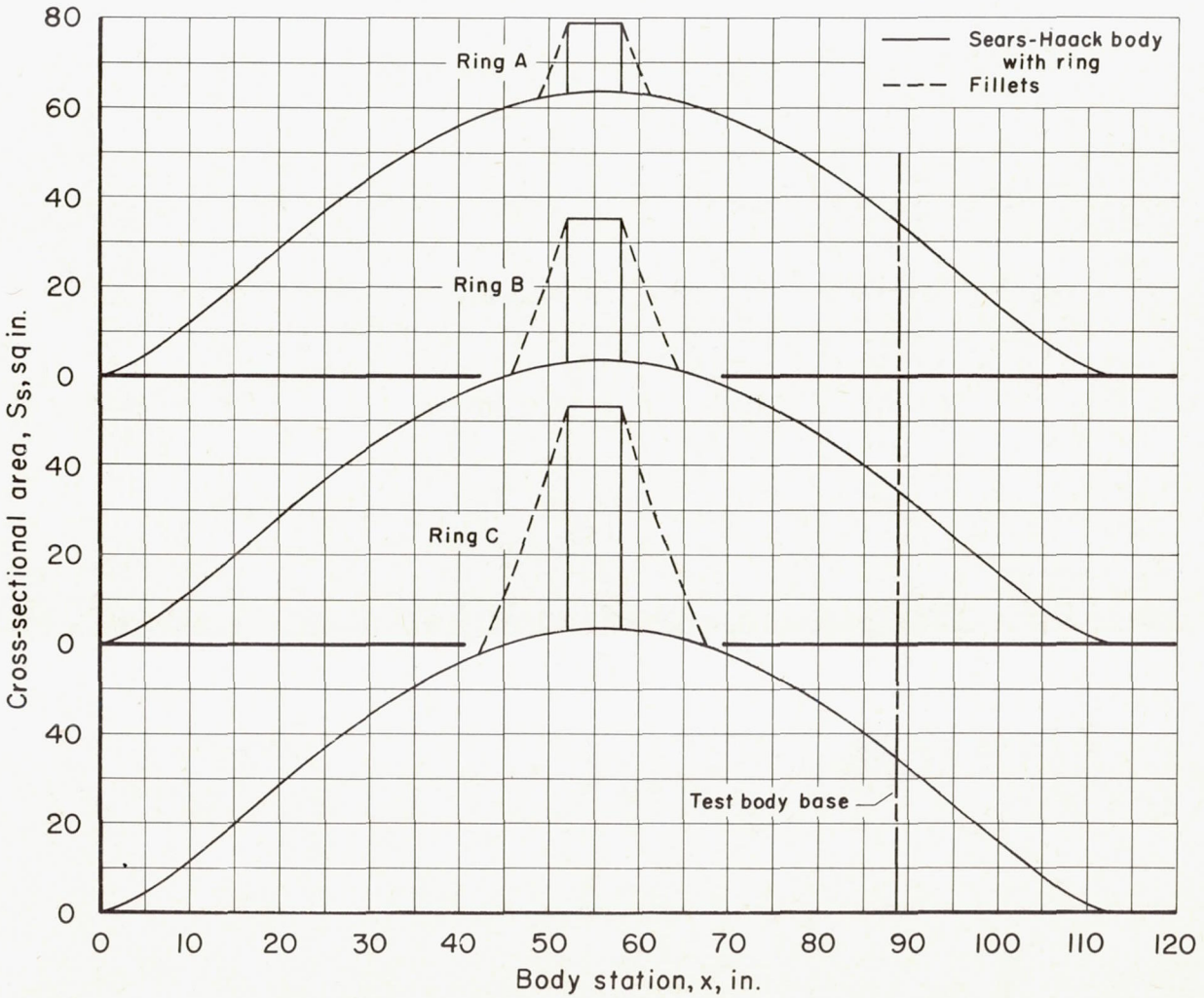

(b) Cross-sectional area distributions (M = 1.00).

Figure 1.- Concluded.

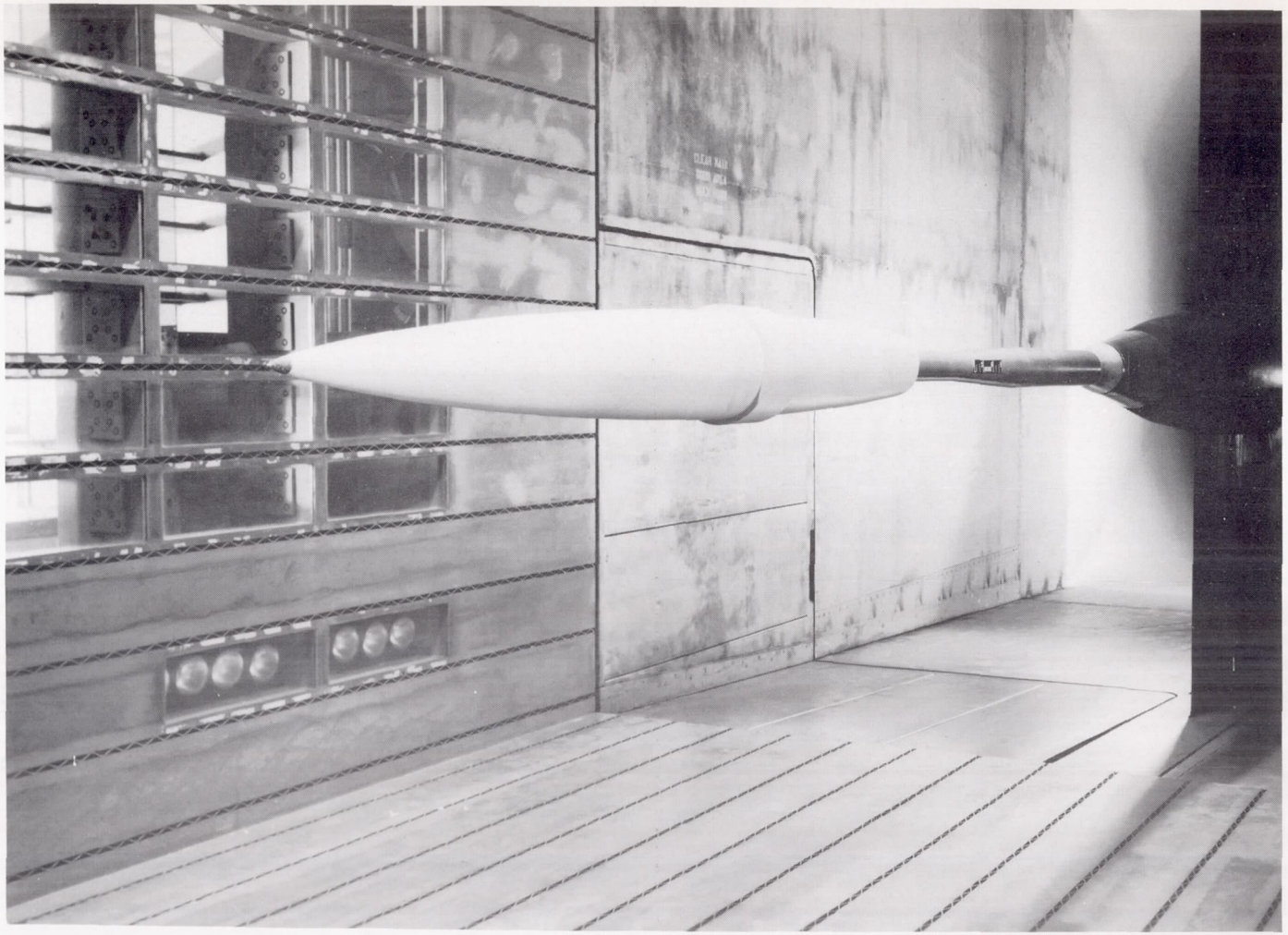

A-21809

Figure 2.- Basic body with ring A (step height 0.5 in.) in the test section of the Ames 14-foot transonic wind tunnel.

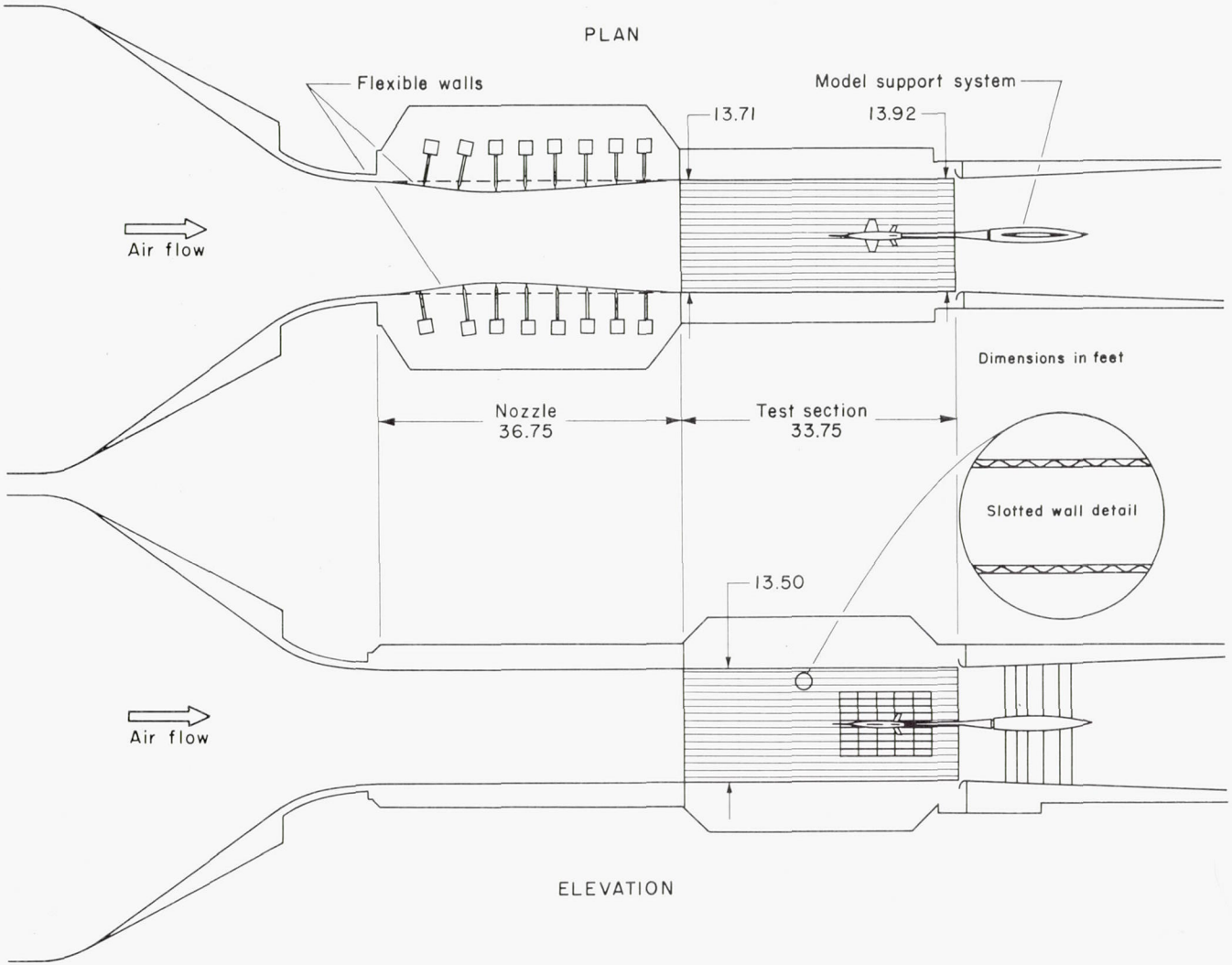

Figure 3.- Two views of the high-speed region of the Ames 14-foot transonic wind tunnel.

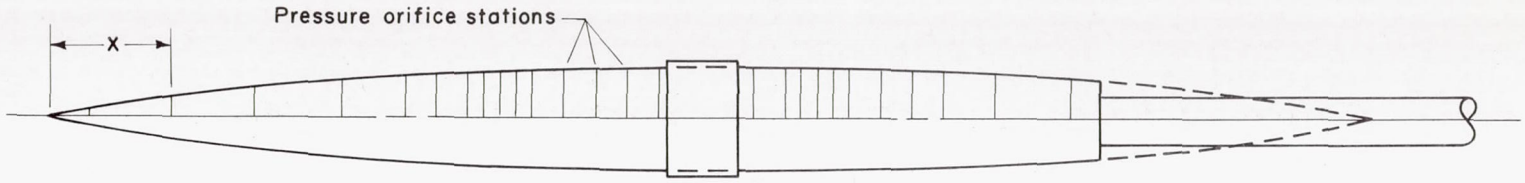

All configurations
$\theta = 0°, 22.5°$, and $90°$

Orifice station	x inches
1	3.50
2	10.50
3	17.50
4	24.90
5	30.28
6	32.96
7	35.65
8	36.99
9	38.33
10	39.67
11	41.01
12	43.70
13	46.38
14	49.07
15	51.75
16	59.81
17	62.49
18	63.84
19	65.18
20	66.52
21	67.86
22	70.55
23	73.23
24	75.92
25	81.29
26	86.66

Additional orifice stations for model with ring A
$\theta = 90°$ only

Orifice station	x inches	
27	50.30	
28	51.05	
29	51.50	
30	51.60	
31	51.70	
32	51.80	
33	51.90	
34	52.00	
35	52.10	
36	52.10	Face of forward step
37	53.10	
38	54.10	Top of cylinder between steps
39	55.10	
40	56.10	
41	57.10	
42	58.10	Face of rearward step
43	58.10	
44	58.20	
45	58.30	
46	58.40	
47	58.50	
48	58.60	
49	58.70	
50	59.15	

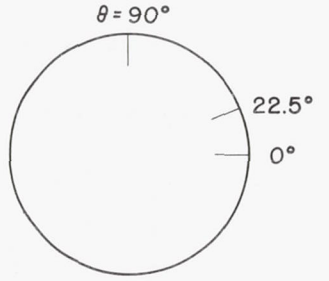

Section showing orifice locations around the body

Figure 4.- Location of pressure orifices on the bodies.

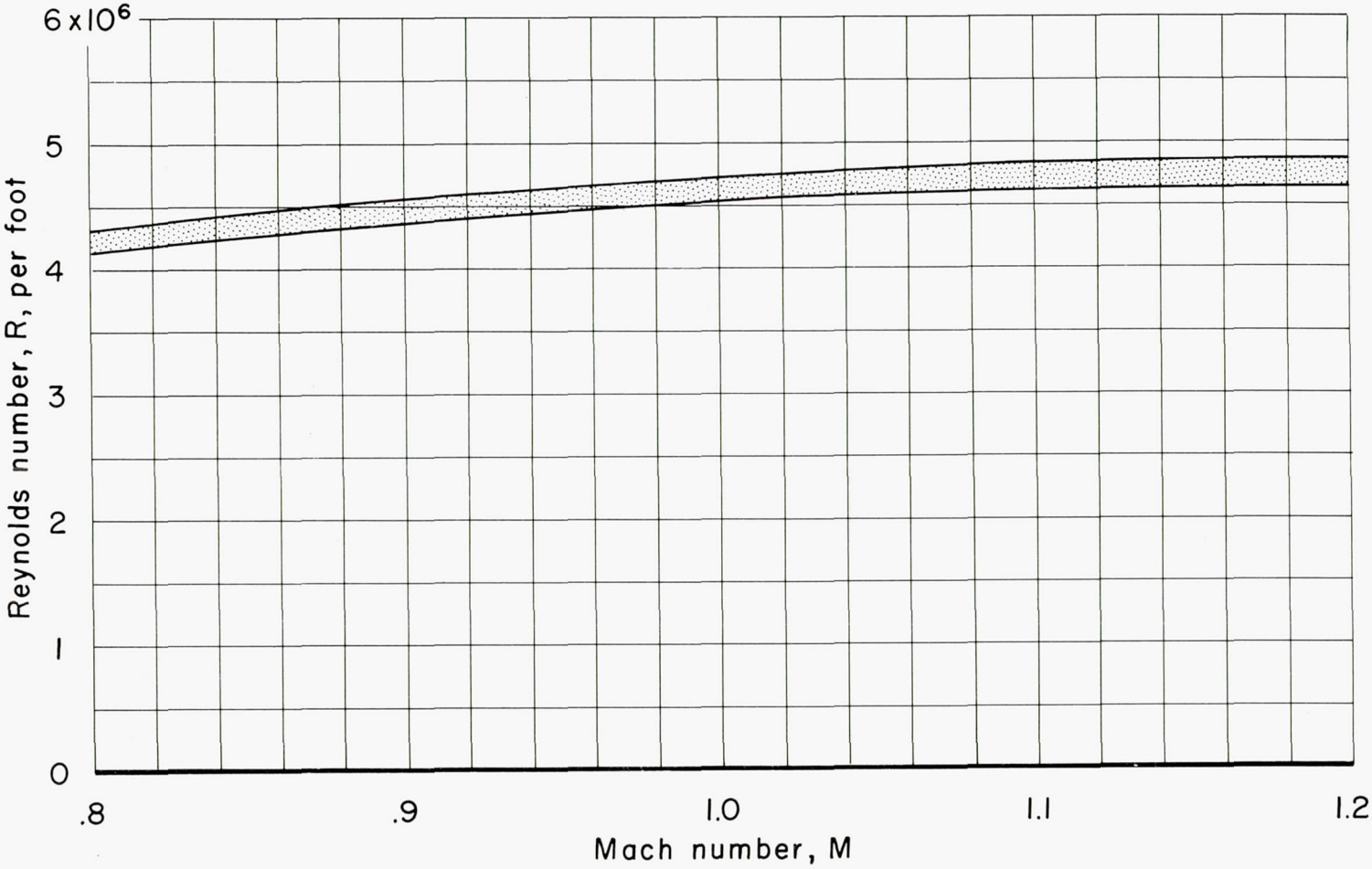

Figure 5.- Reynolds number per foot envelope curve for all the tests.

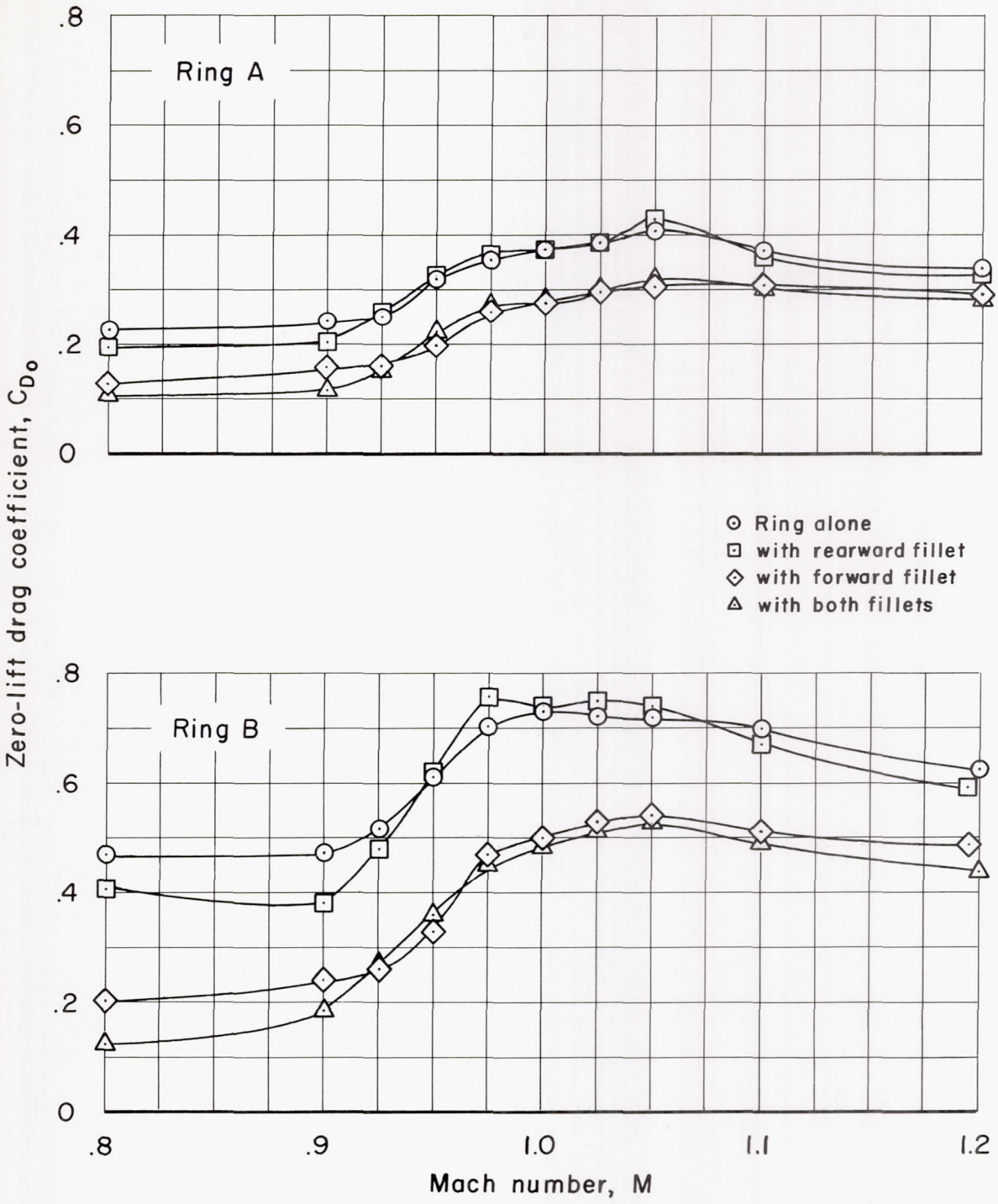

(a) Ring A and Ring B.

Figure 6.- Zero-lift drag coefficients for the basic body with various rings and fillet combinations.

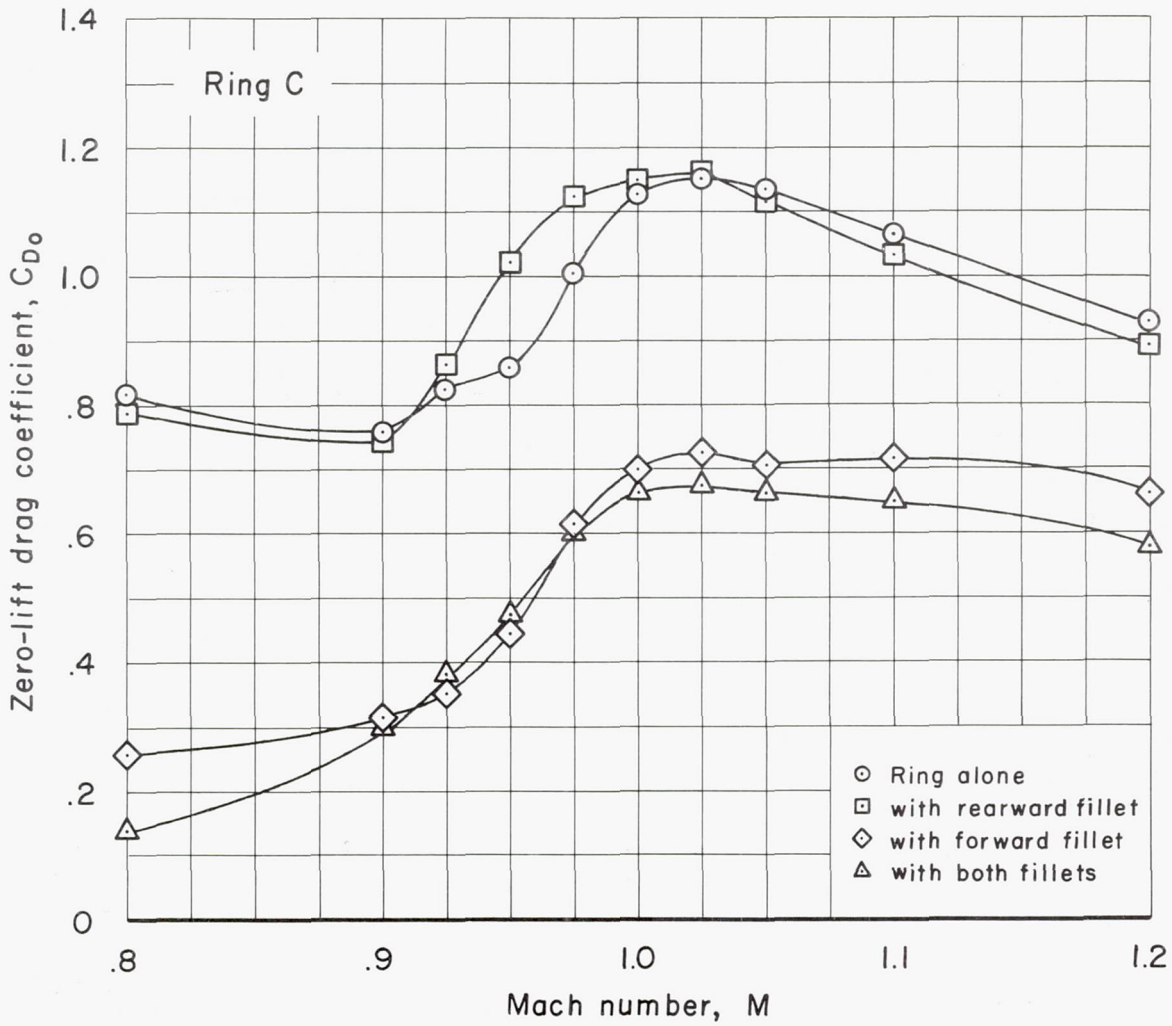

(b) Ring C.

Figure 6.- Concluded.

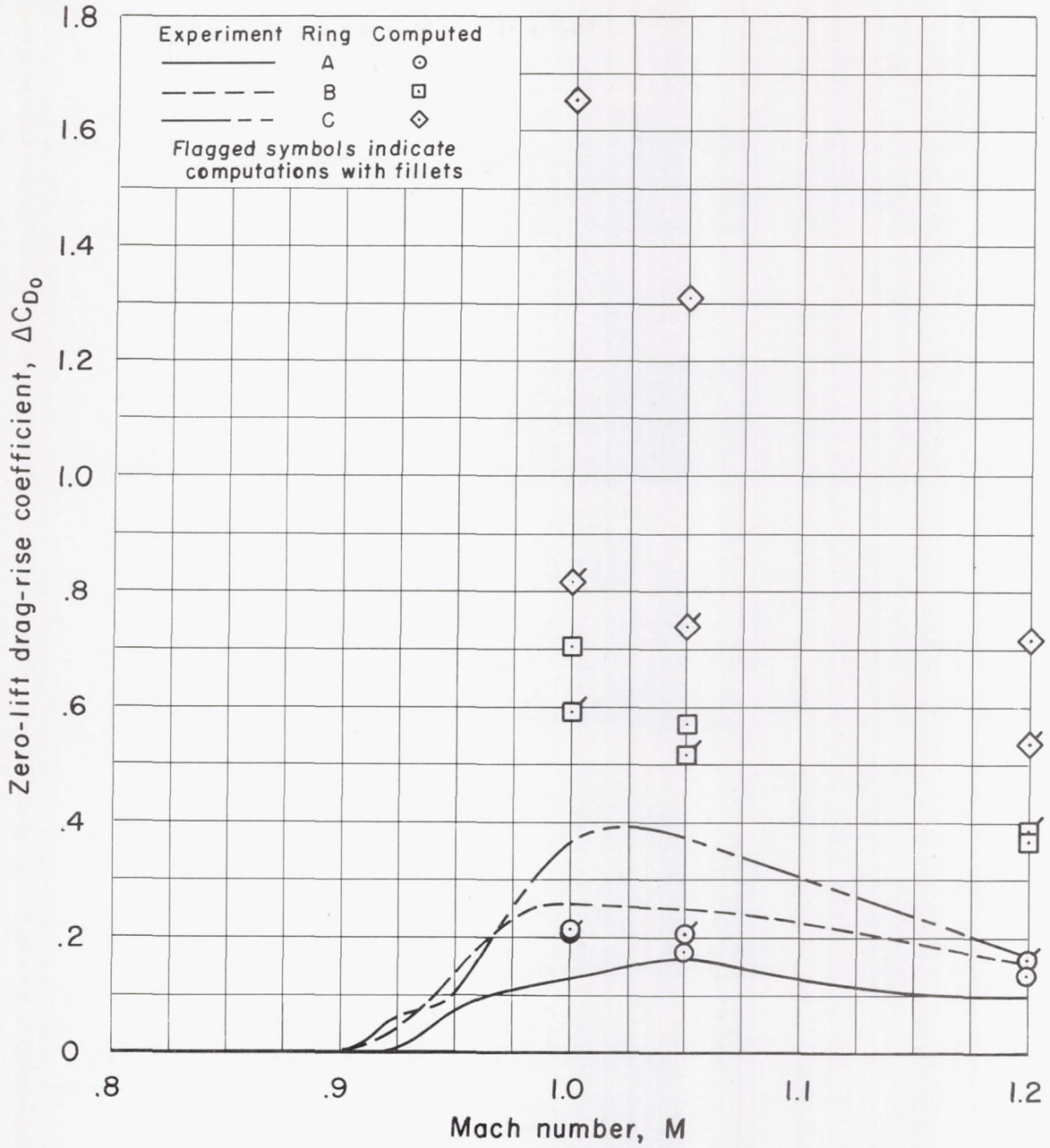

Figure 7.- Zero-lift drag-rise coefficients for the ring-body models and wave-drag coefficients computed by means of 25 harmonics.

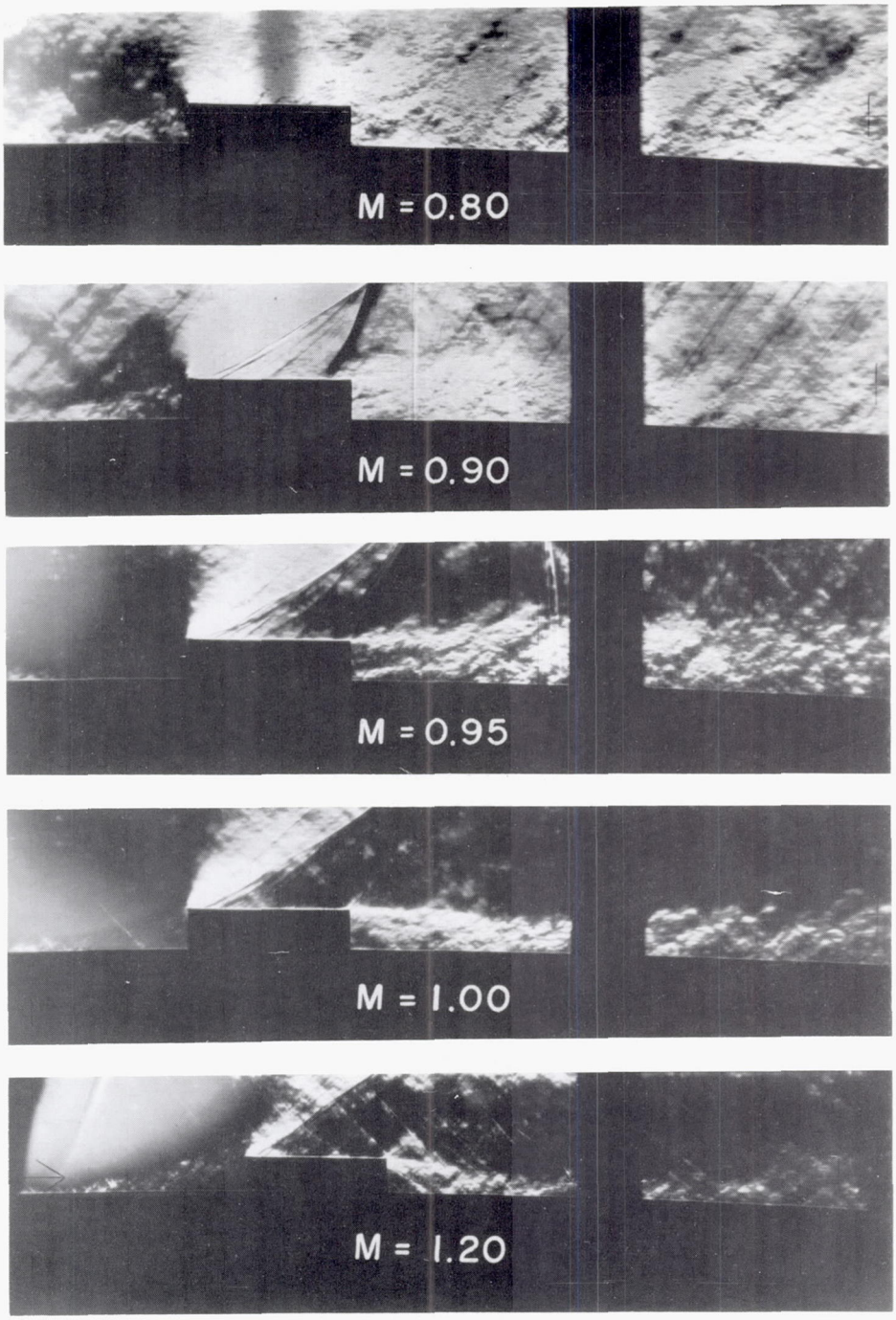

(a) Without fillets.

Figure 8.- Schlieren pictures of the air flow over ring C with and without 10° fillets (step height 1.5 in.).

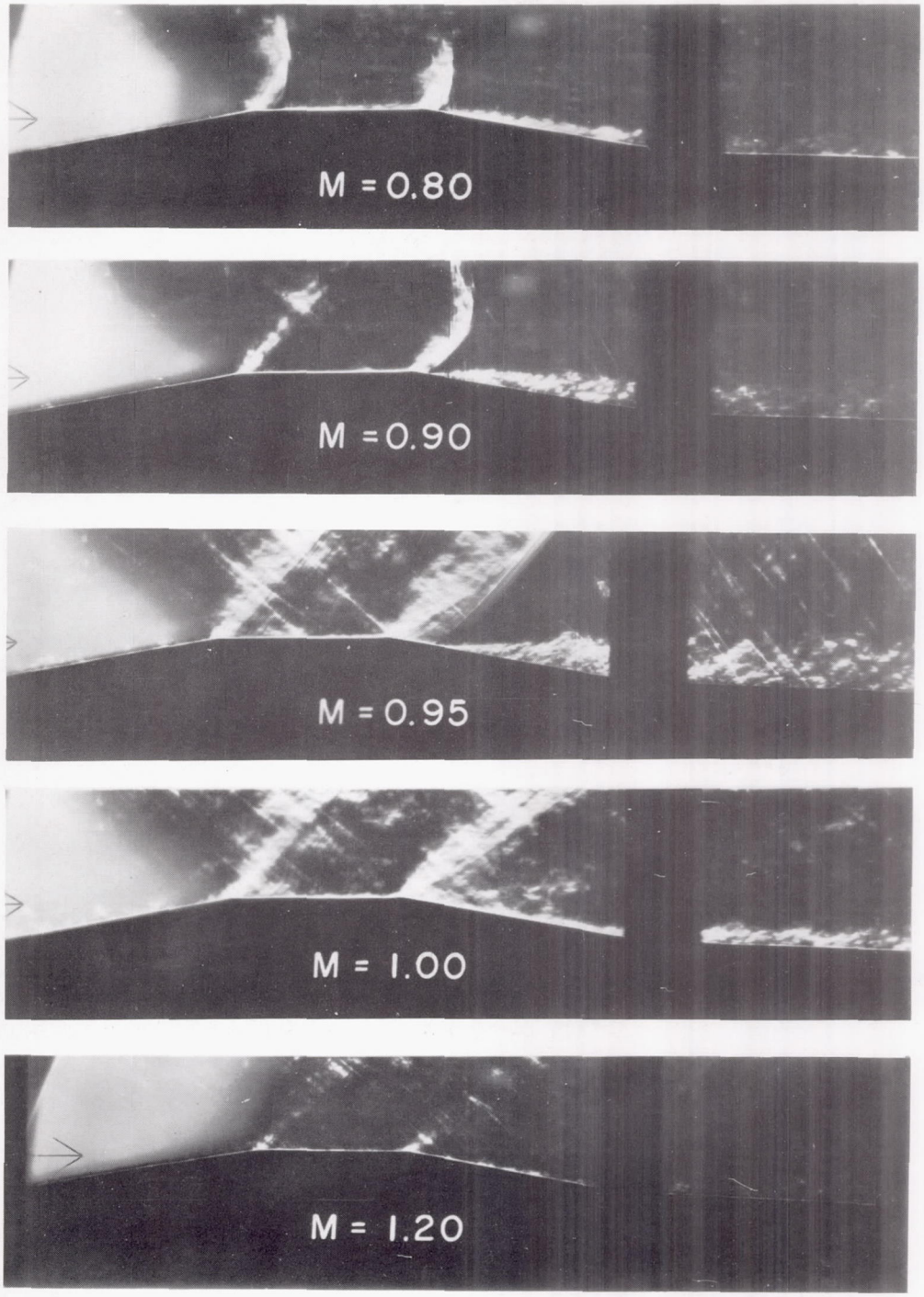

(b) With both fillets.

Figure 8.- Continued.

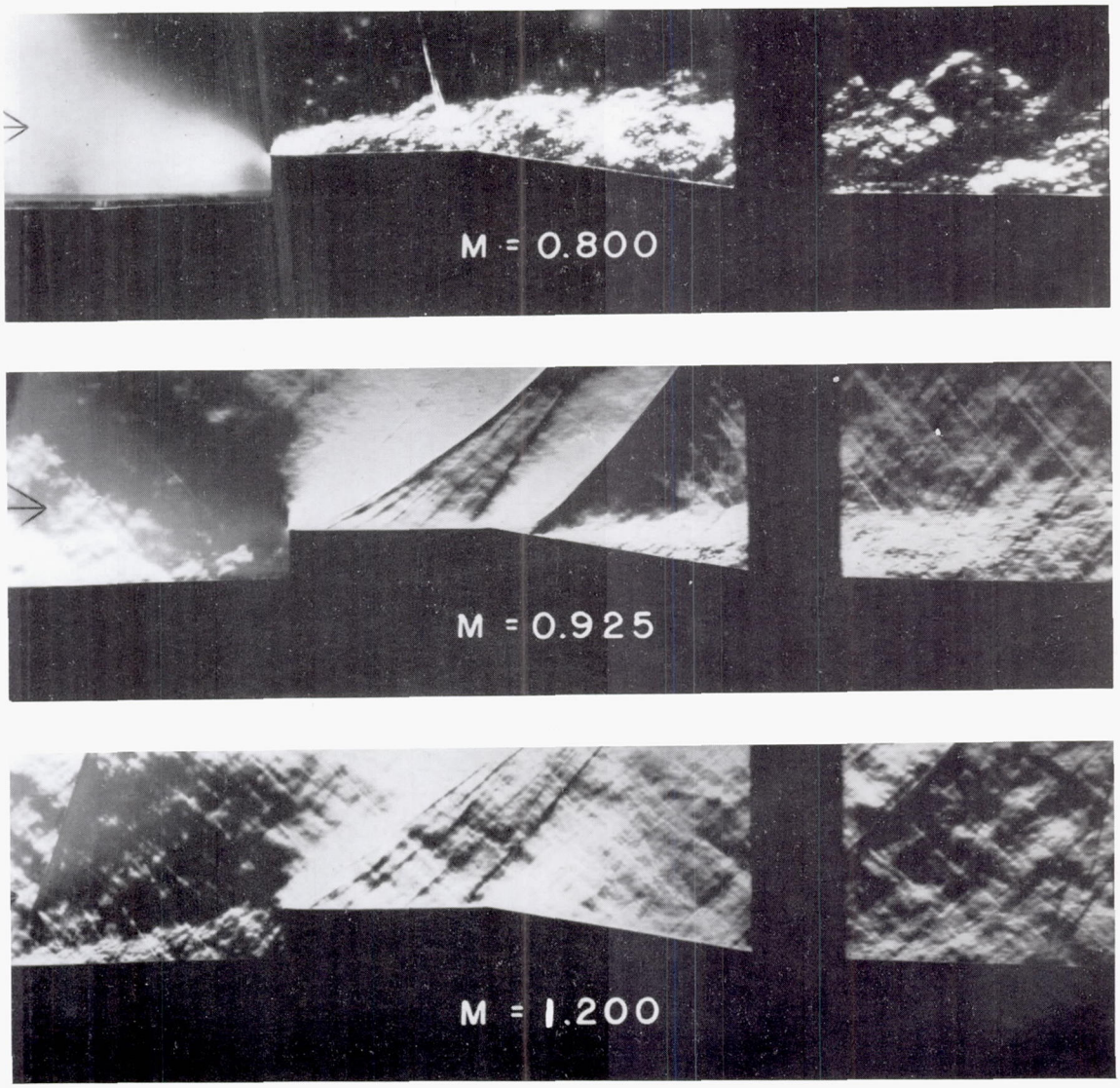

(c) With rearward fillet.

Figure 8.- Continued.

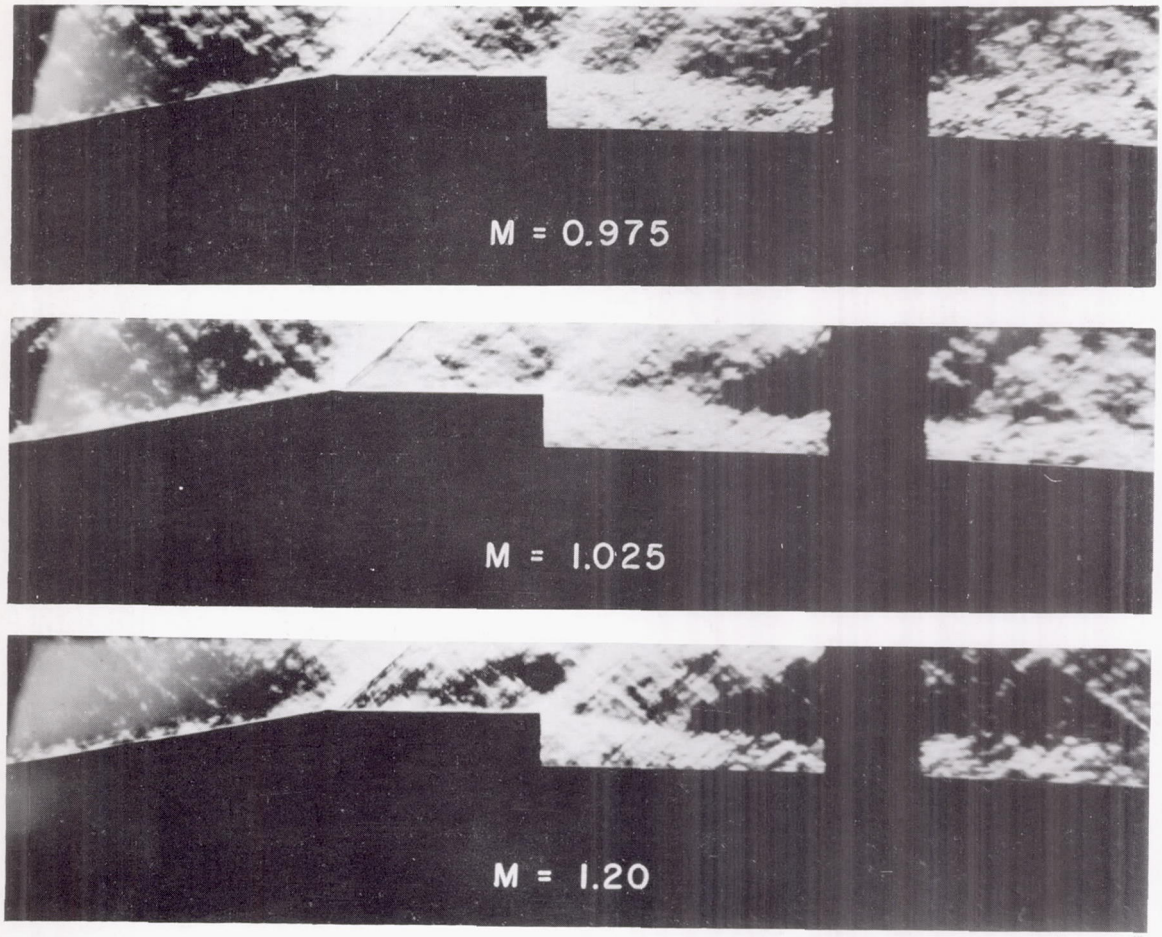

(d) With forward fillet.

Figure 8.- Concluded.

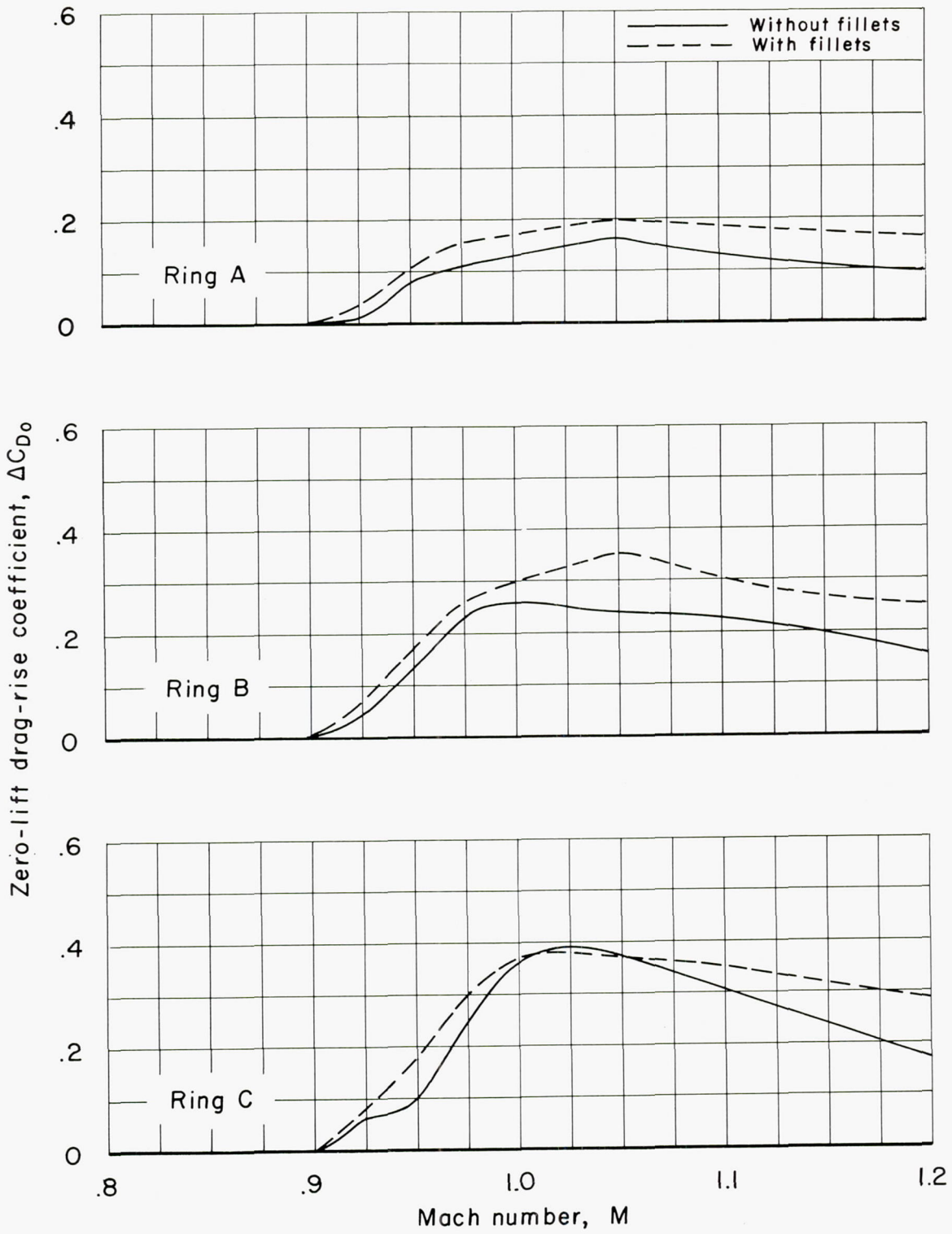

Figure 9.- Zero-lift drag-rise coefficients for the ring-body models with and without the 10° fillets.

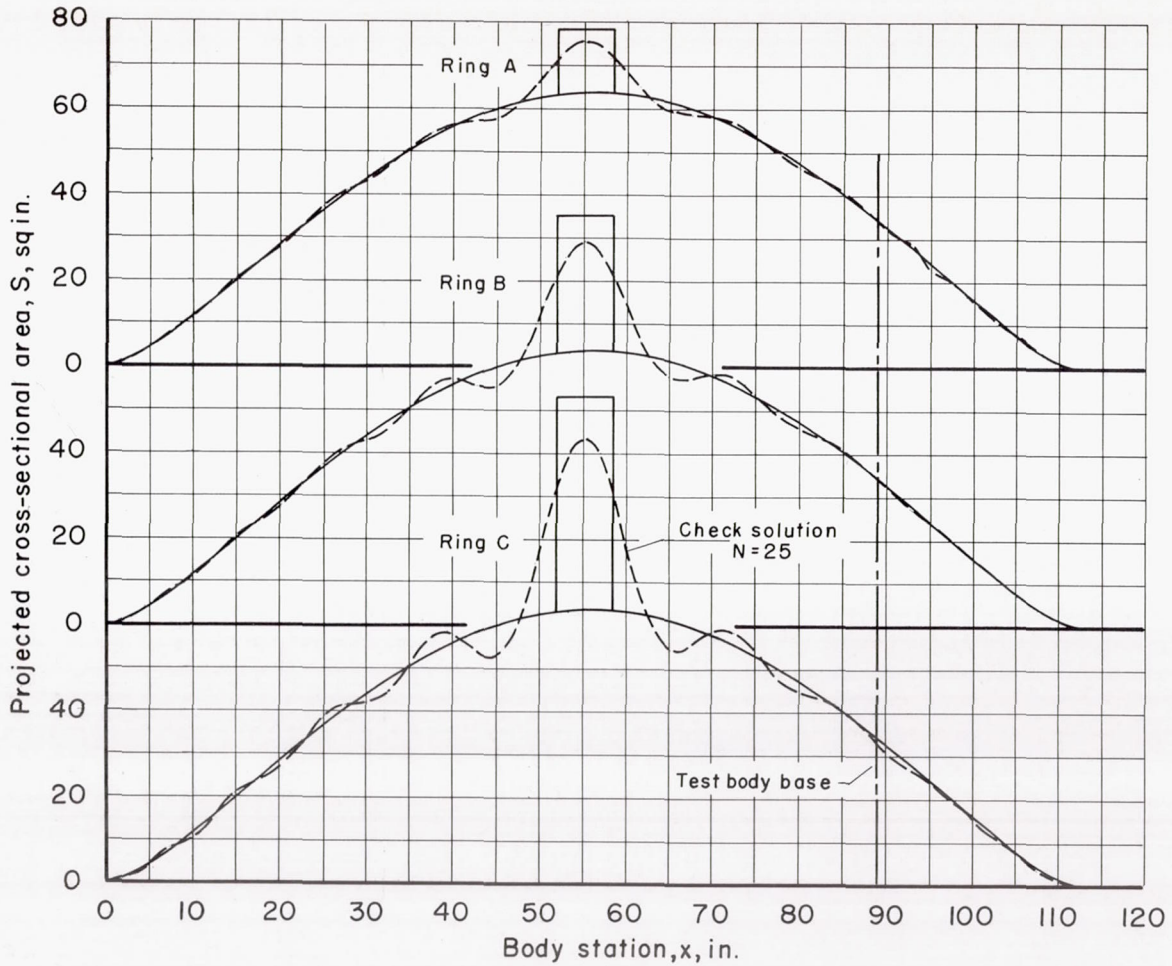

(a) M = 1.00

Figure 10.- Theoretical check solutions for N = 25 in comparison with the given area distributions for ring-body models.

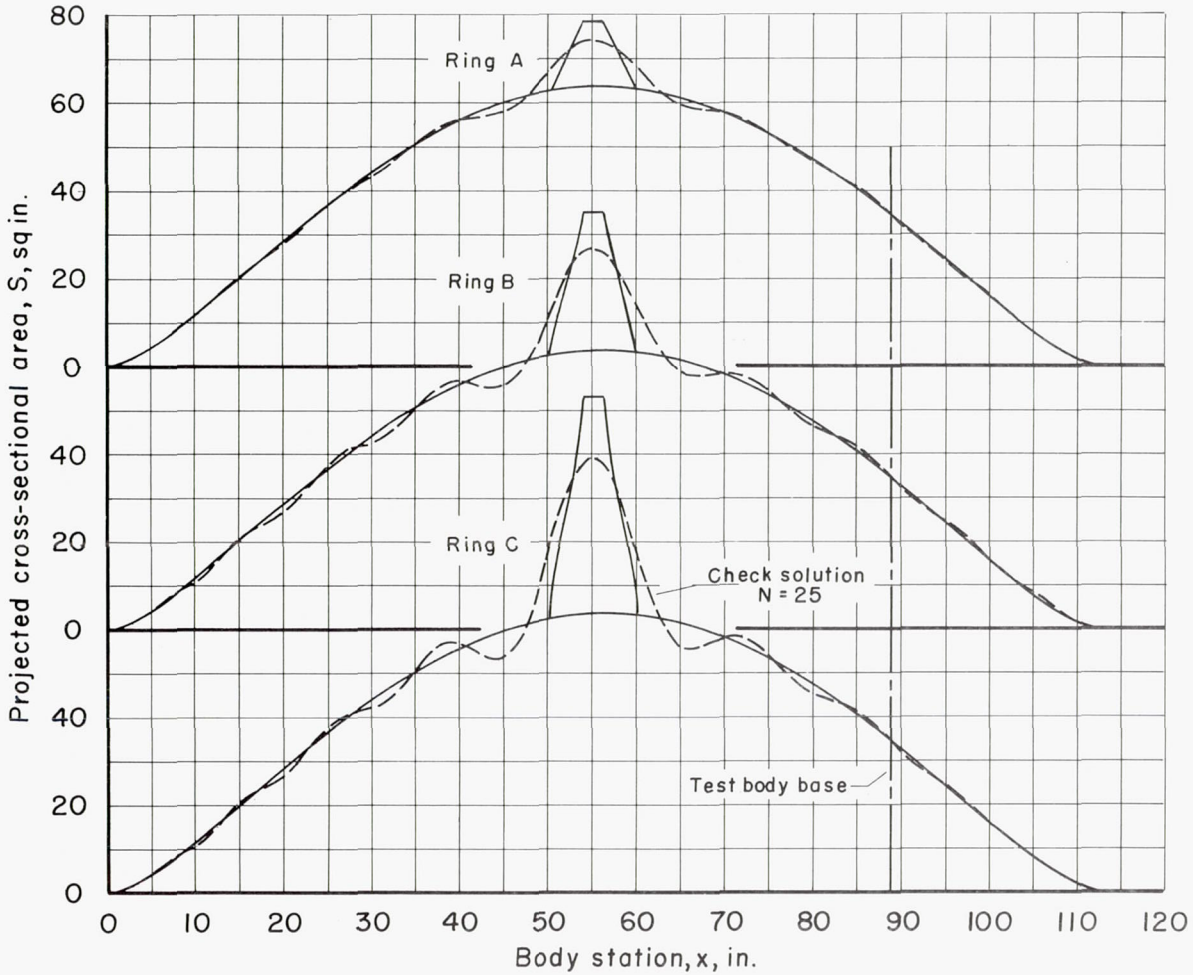

(b) M = 1.05

Figure 10.- Continued.

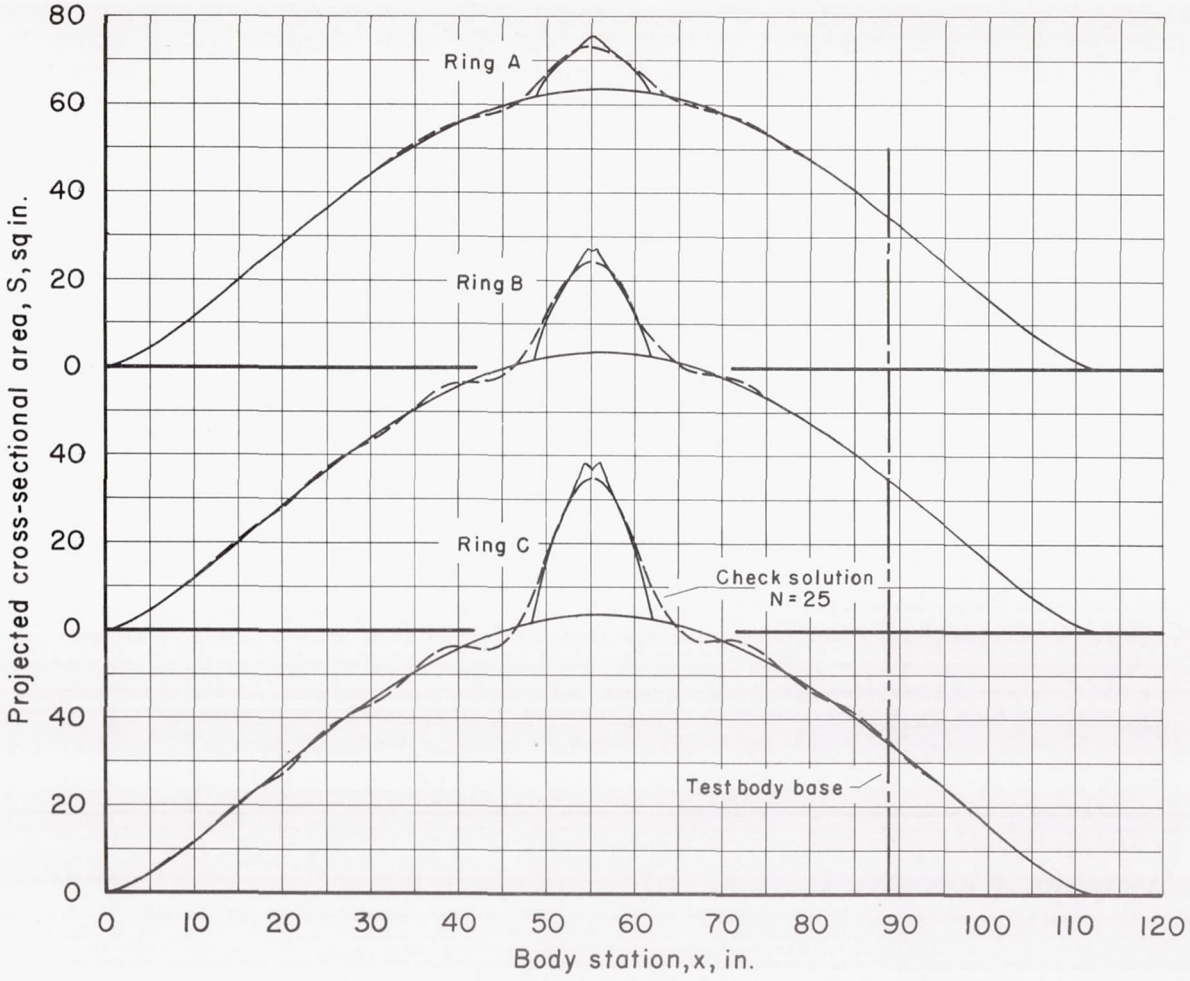

(c) M = 1.20

Figure 10.- Concluded.

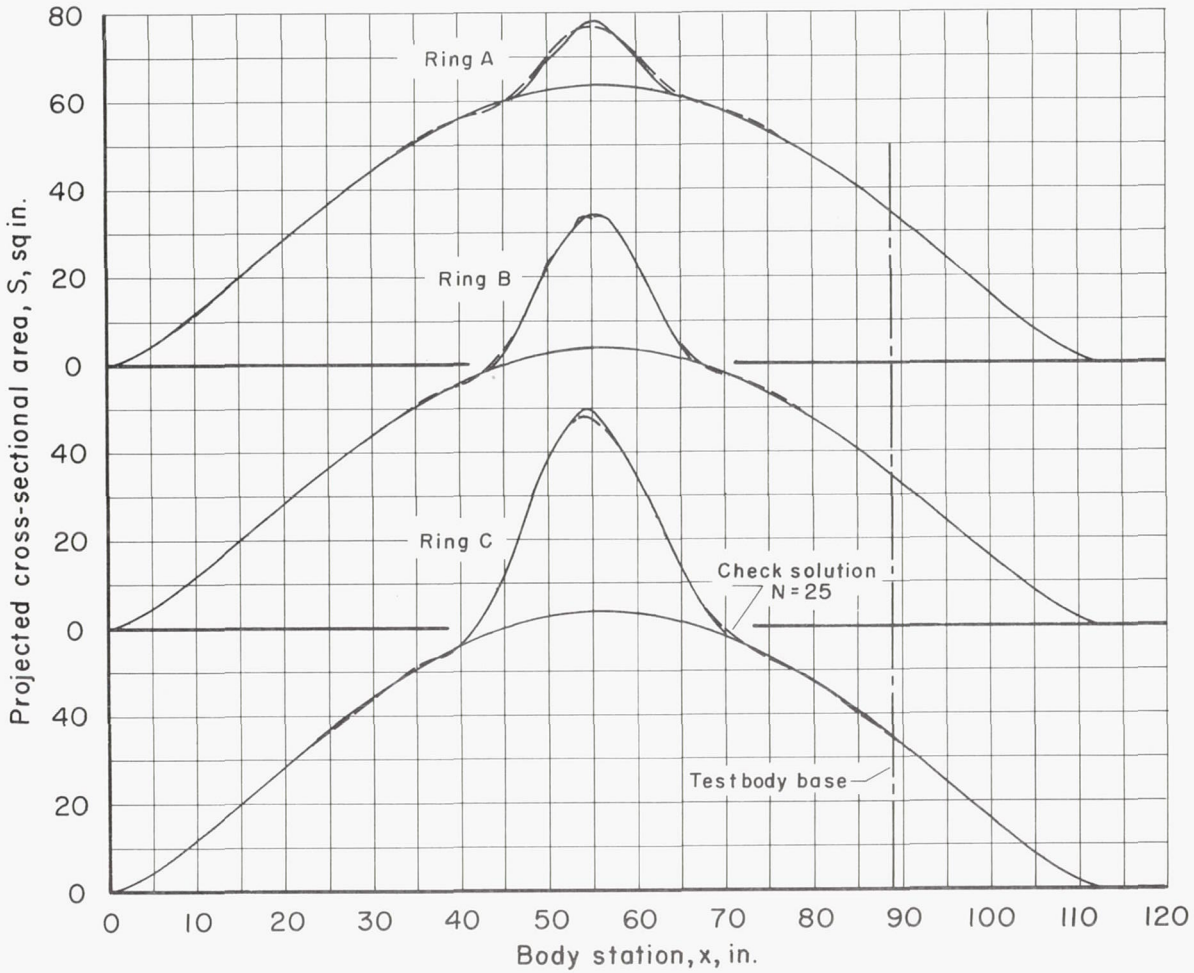

Figure 11.- Theoretical check solutions for N = 25 in comparison with the given area distributions for M = 1.20 for the ring-body models with forward and rearward fillets.

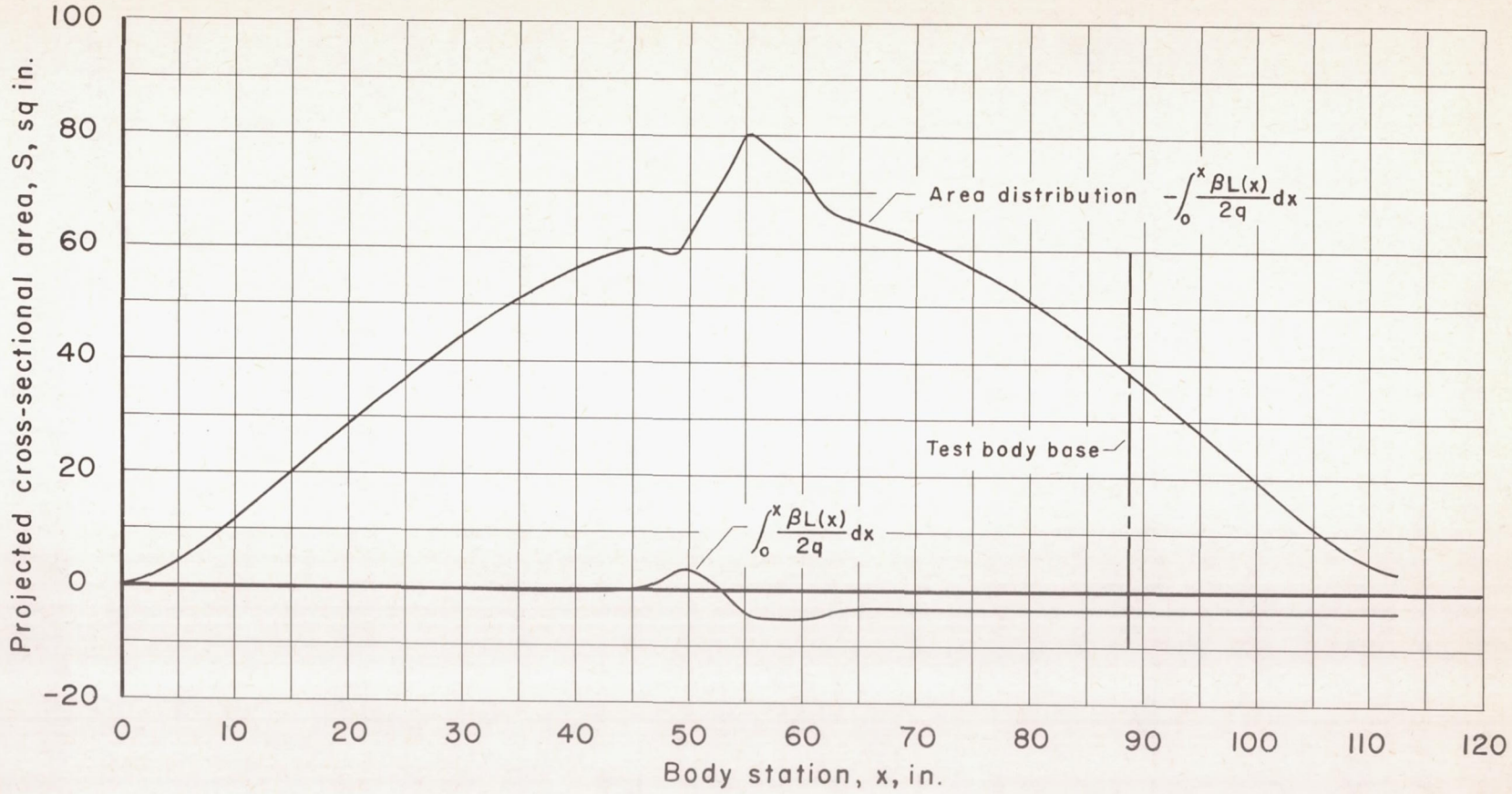

Figure 12.- Equivalent area curve based on the more complete wave-drag equation of reference 3 for the Sears-Haack body with ring A (M = 1.20).

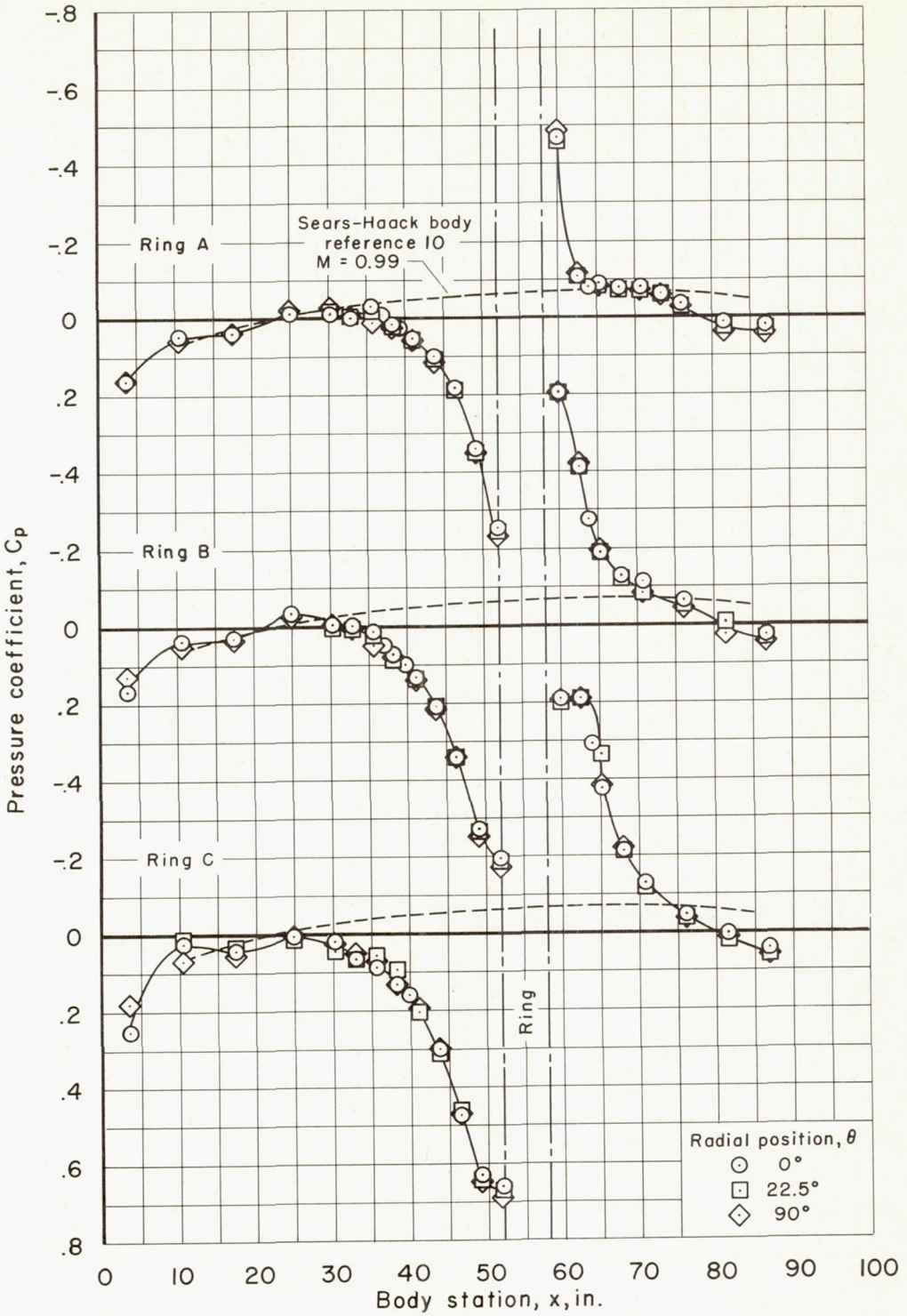

Figure 13.- Surface pressure coefficients of the ring-body models at M = 1.00.

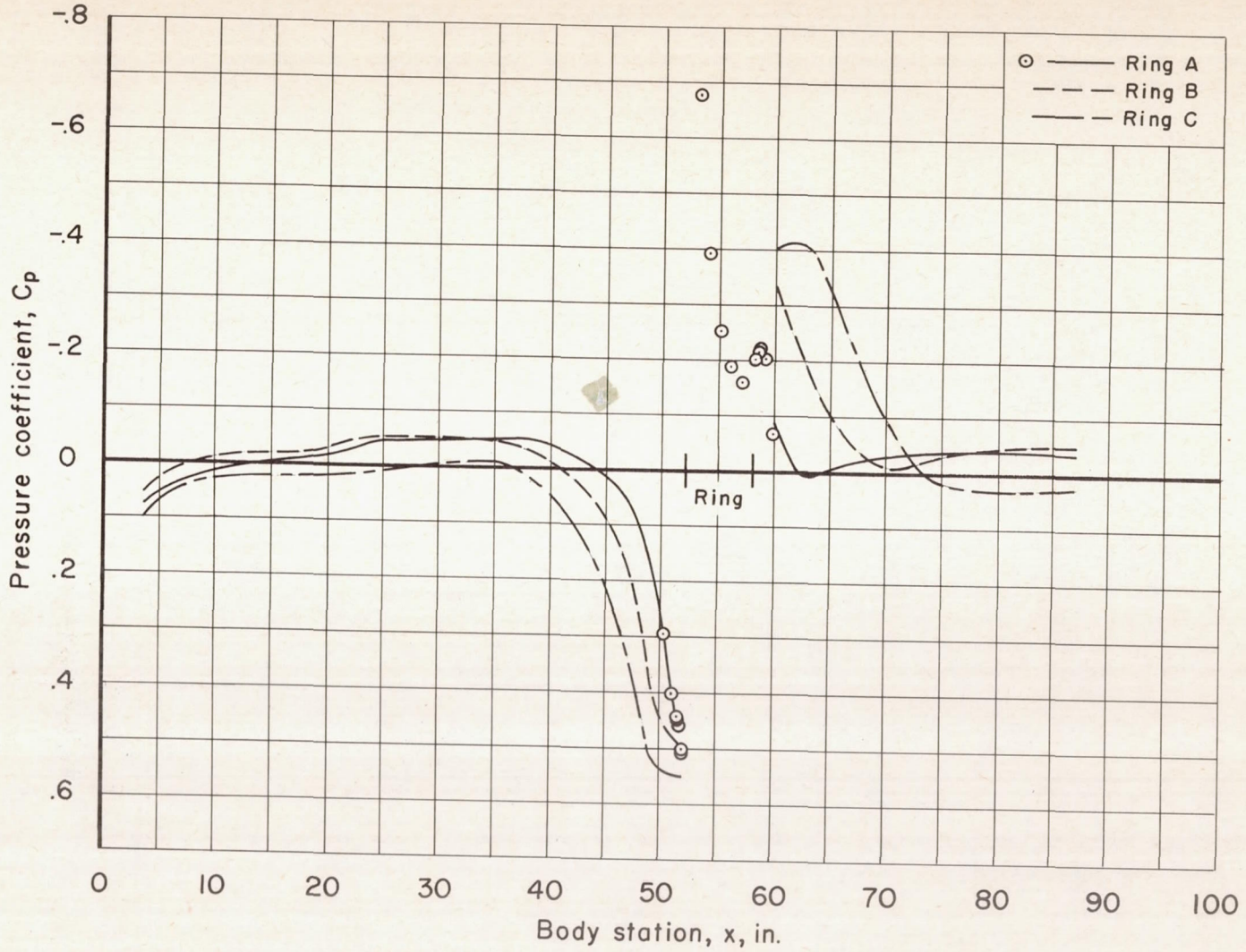

(a) M = 0.80

Figure 14.- Surface pressure coefficients for the ring-body models at various test Mach numbers.

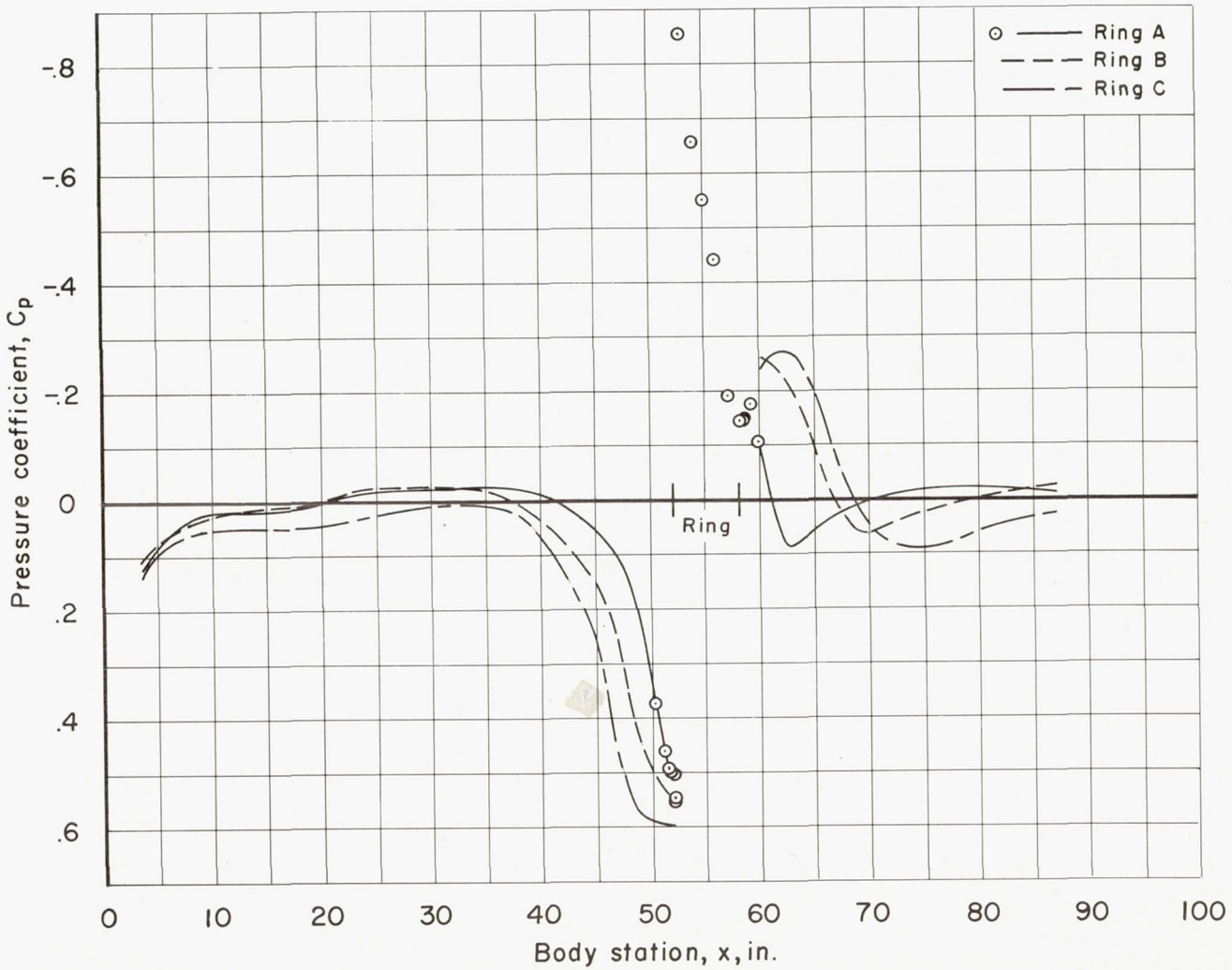

(b) M = 0.90

Figure 14.- Continued.

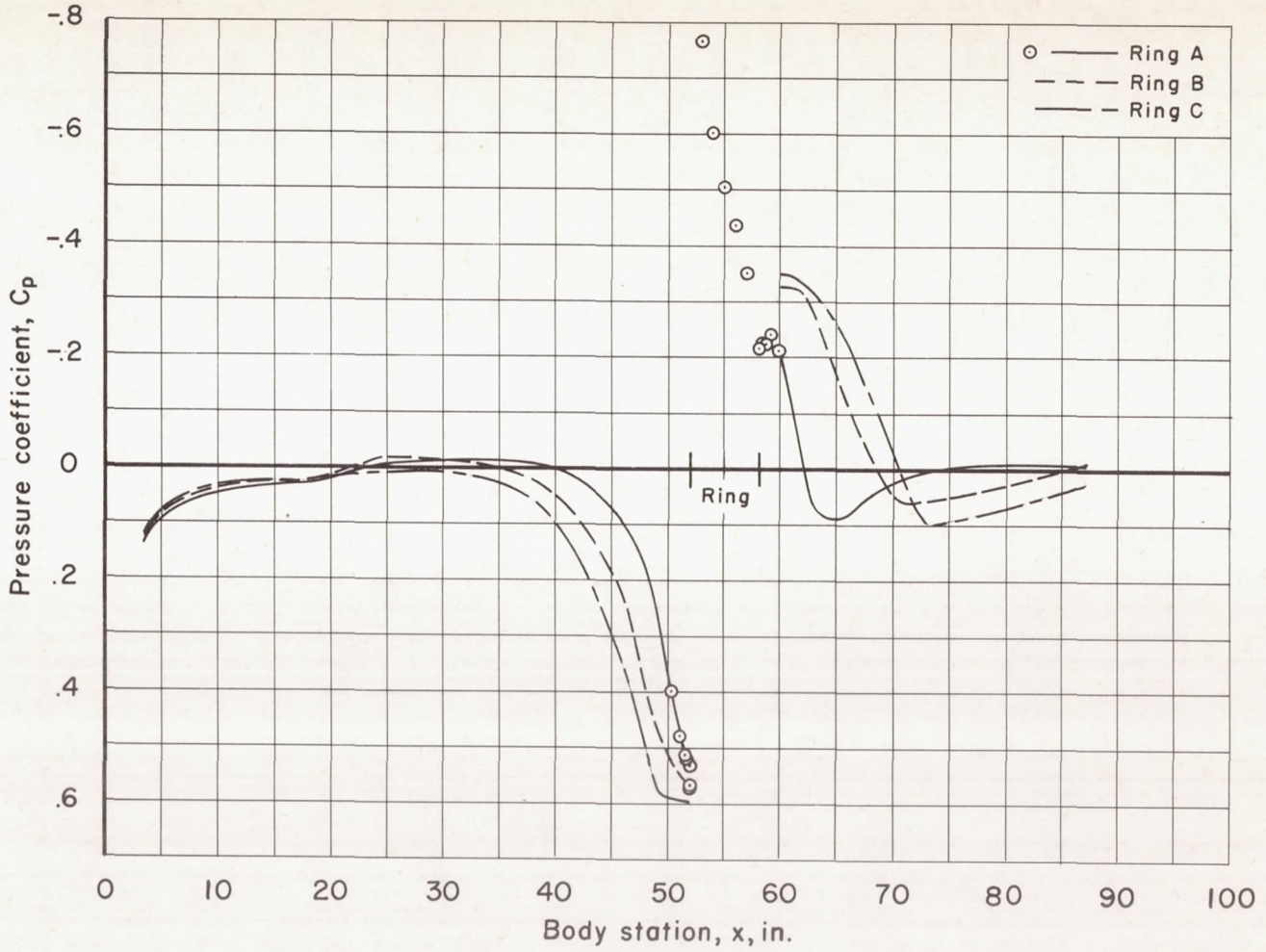

(c) M = 0.925

Figure 14.- Continued.

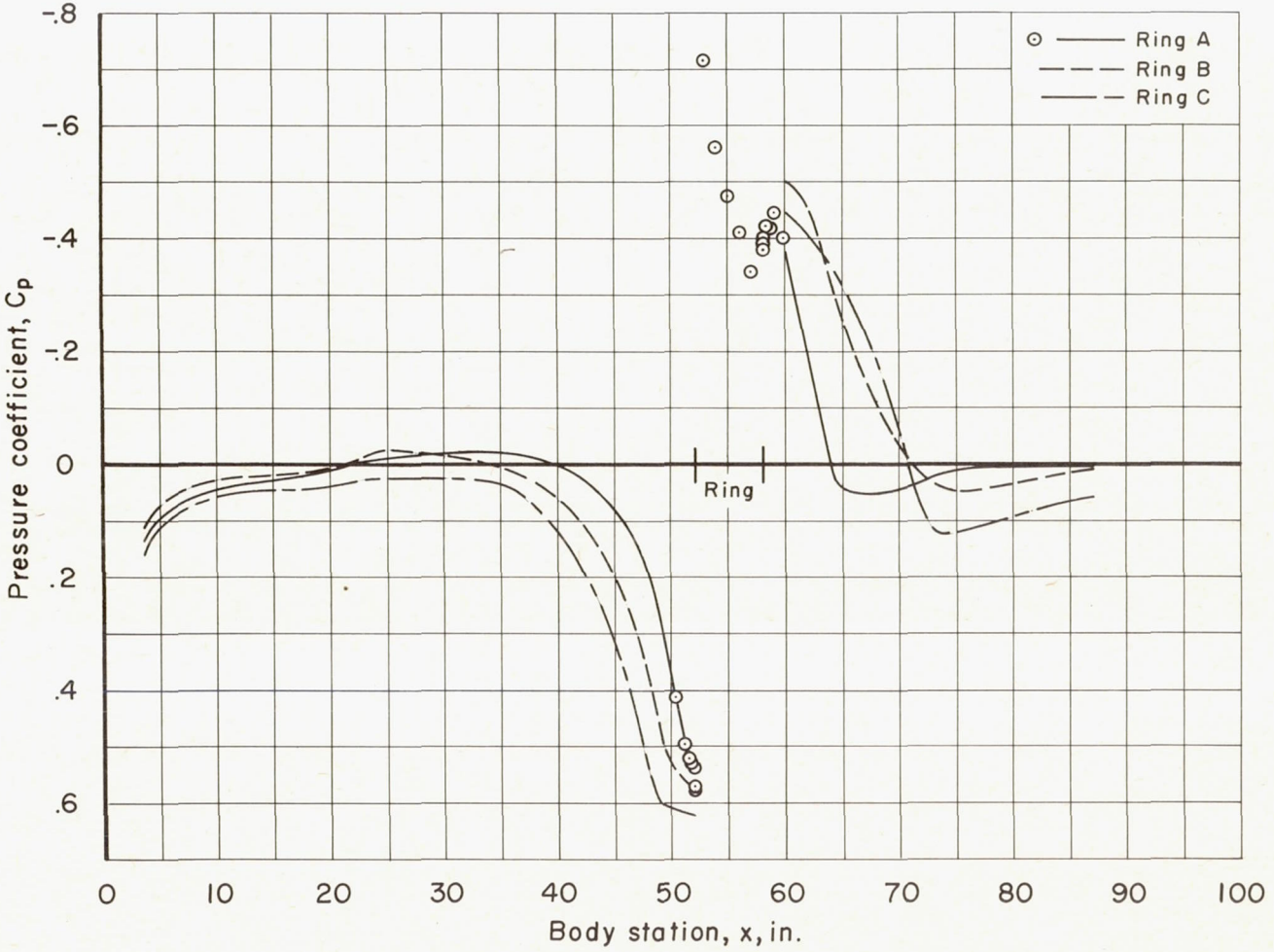

(d) M = 0.95

Figure 14.- Continued.

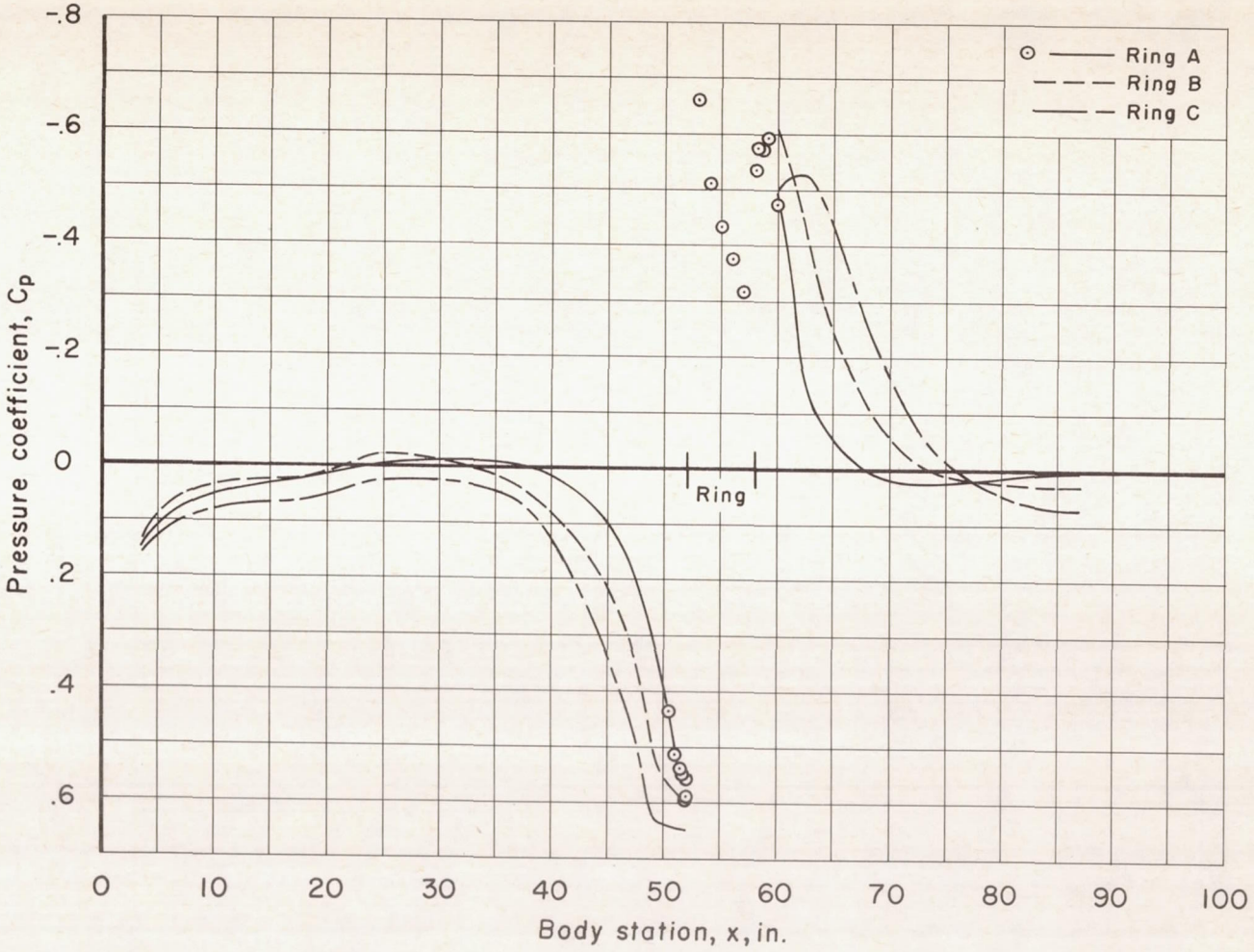

(e) M = 0.975

Figure 14.- Continued.

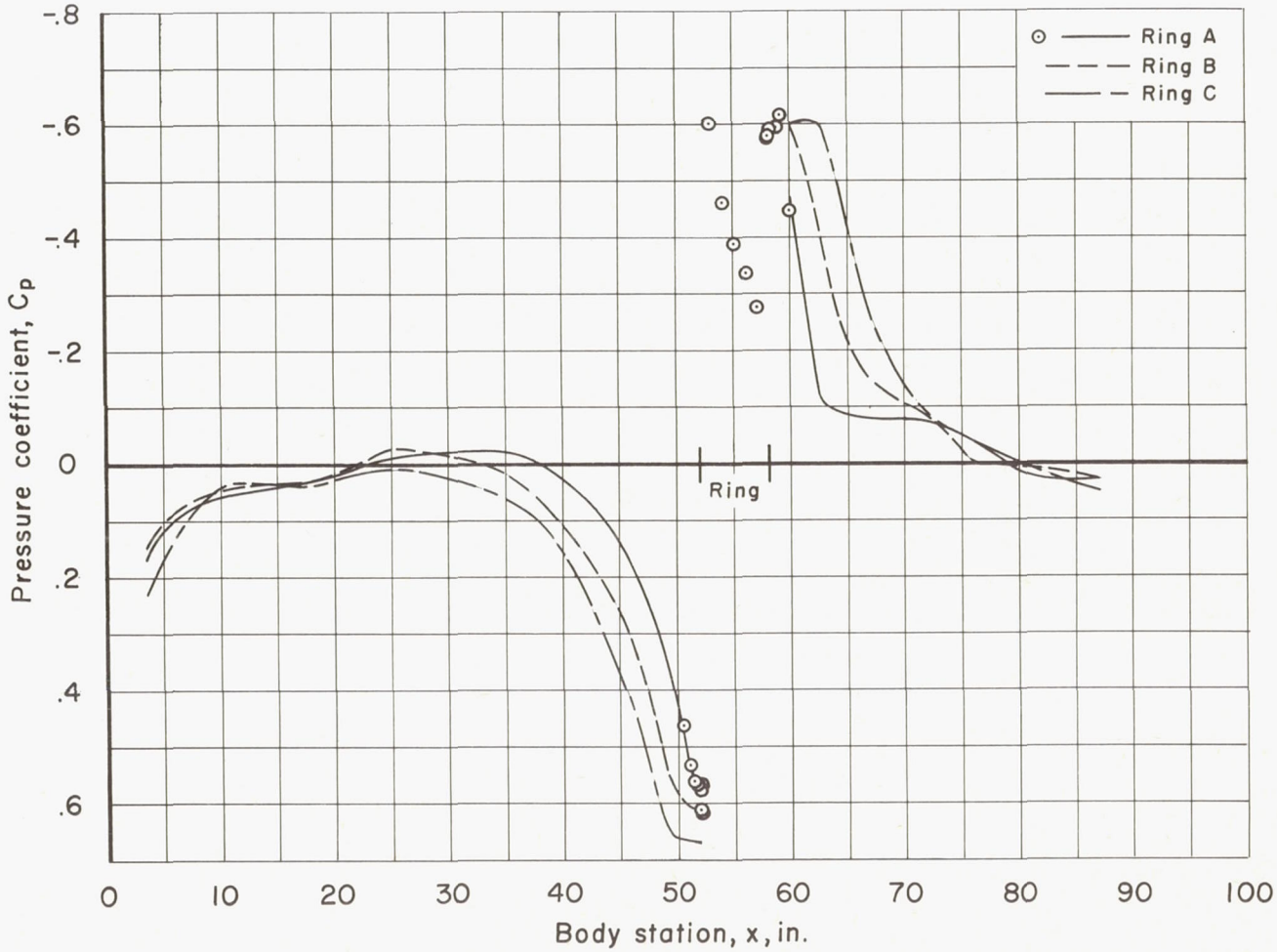

(f) M = 1.00

Figure 14.- Continued.

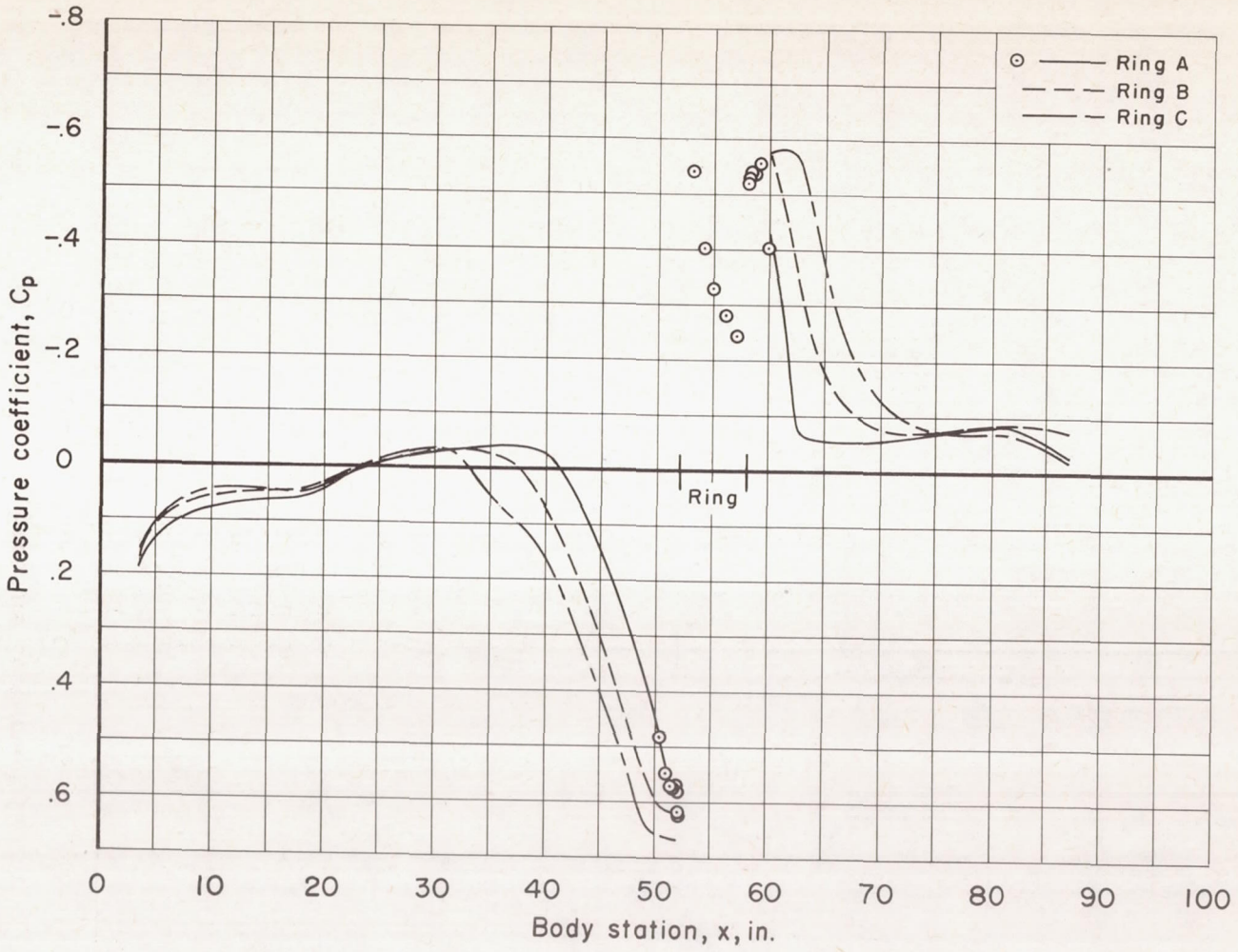

(g) M = 1.025

Figure 14.- Continued.

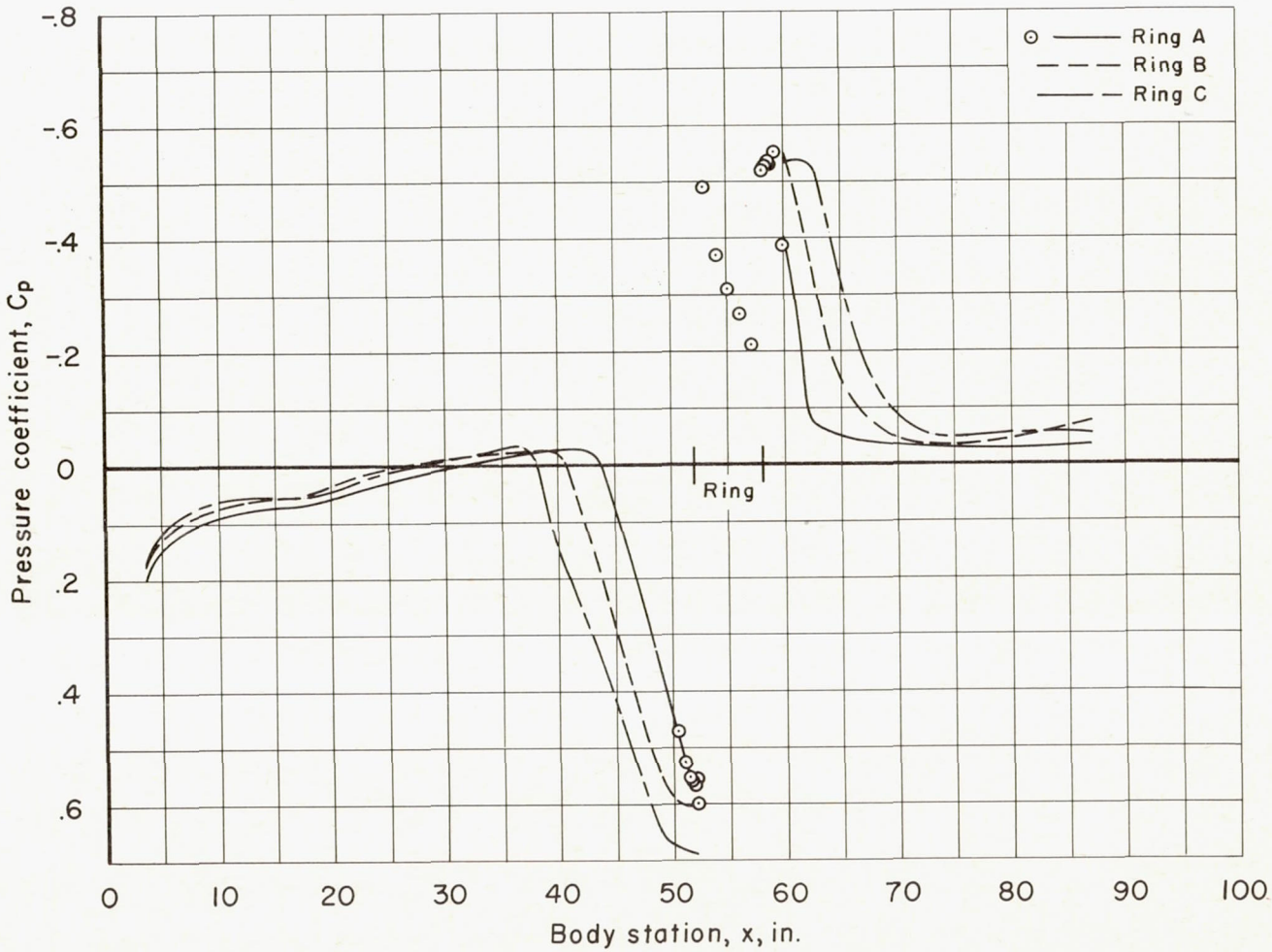

(h) M = 1.05

Figure 14.- Continued.

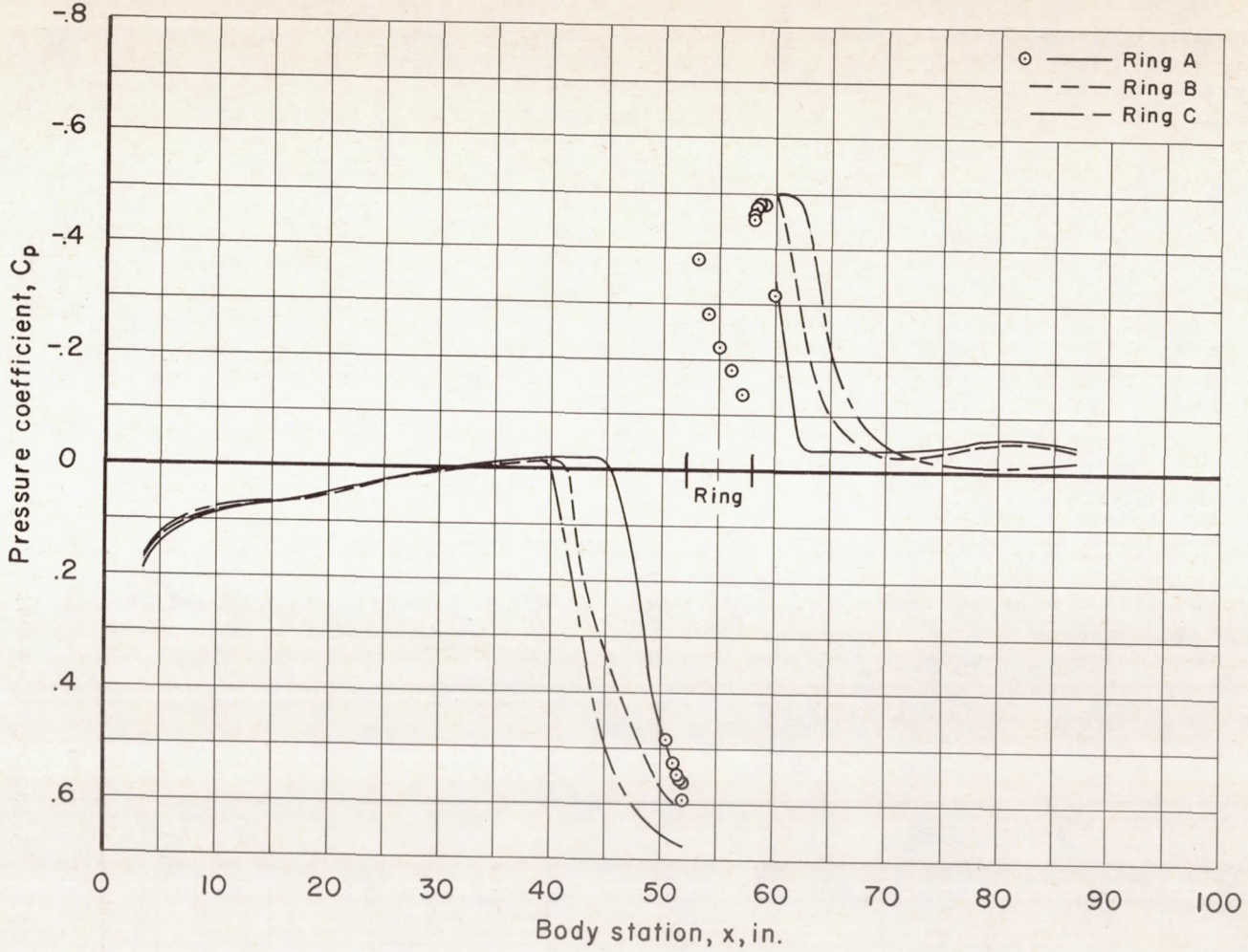

(i) M = 1.10

Figure 14.- Continued.

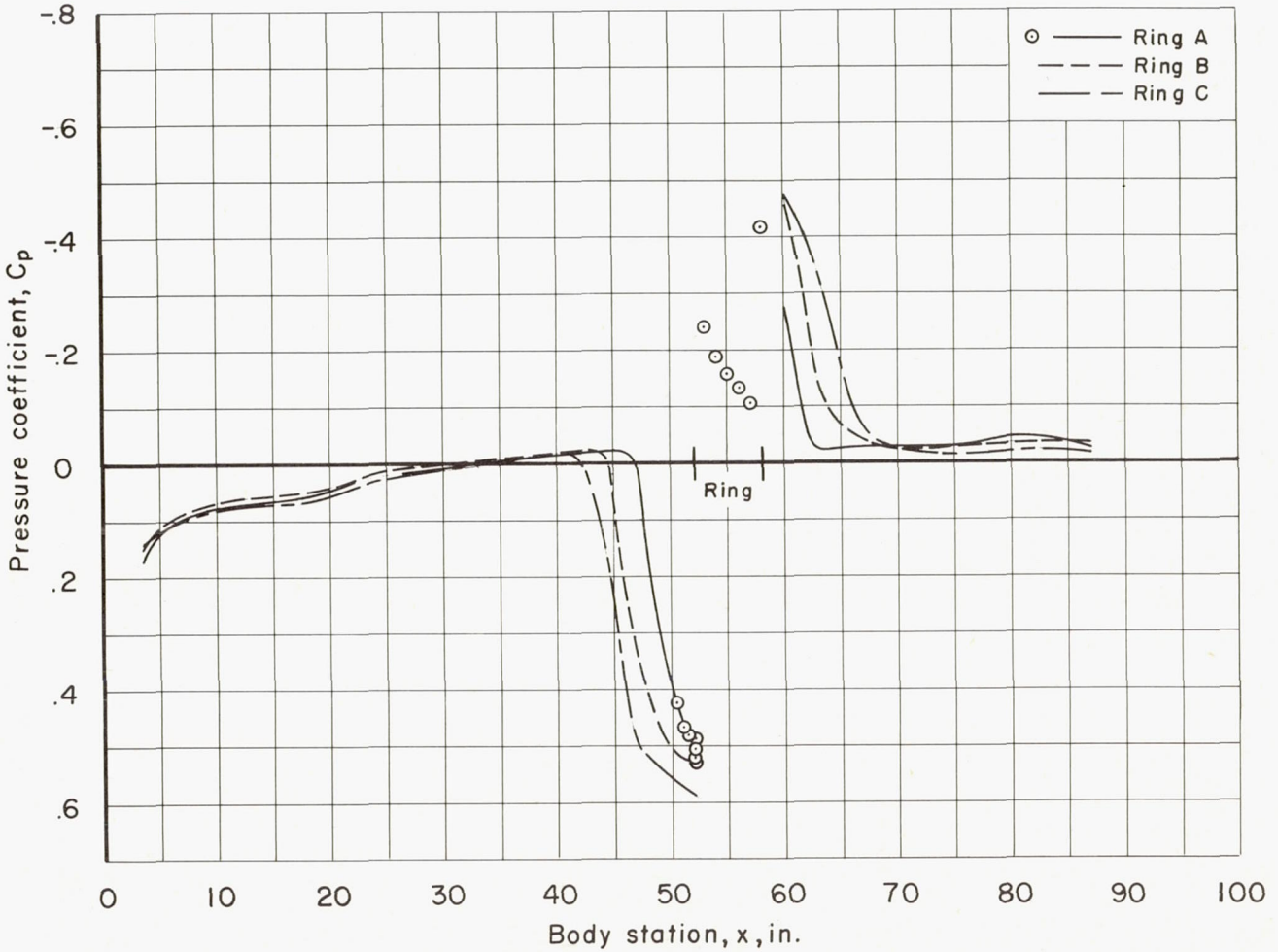

(j) M = 1.20

Figure 14.- Concluded.

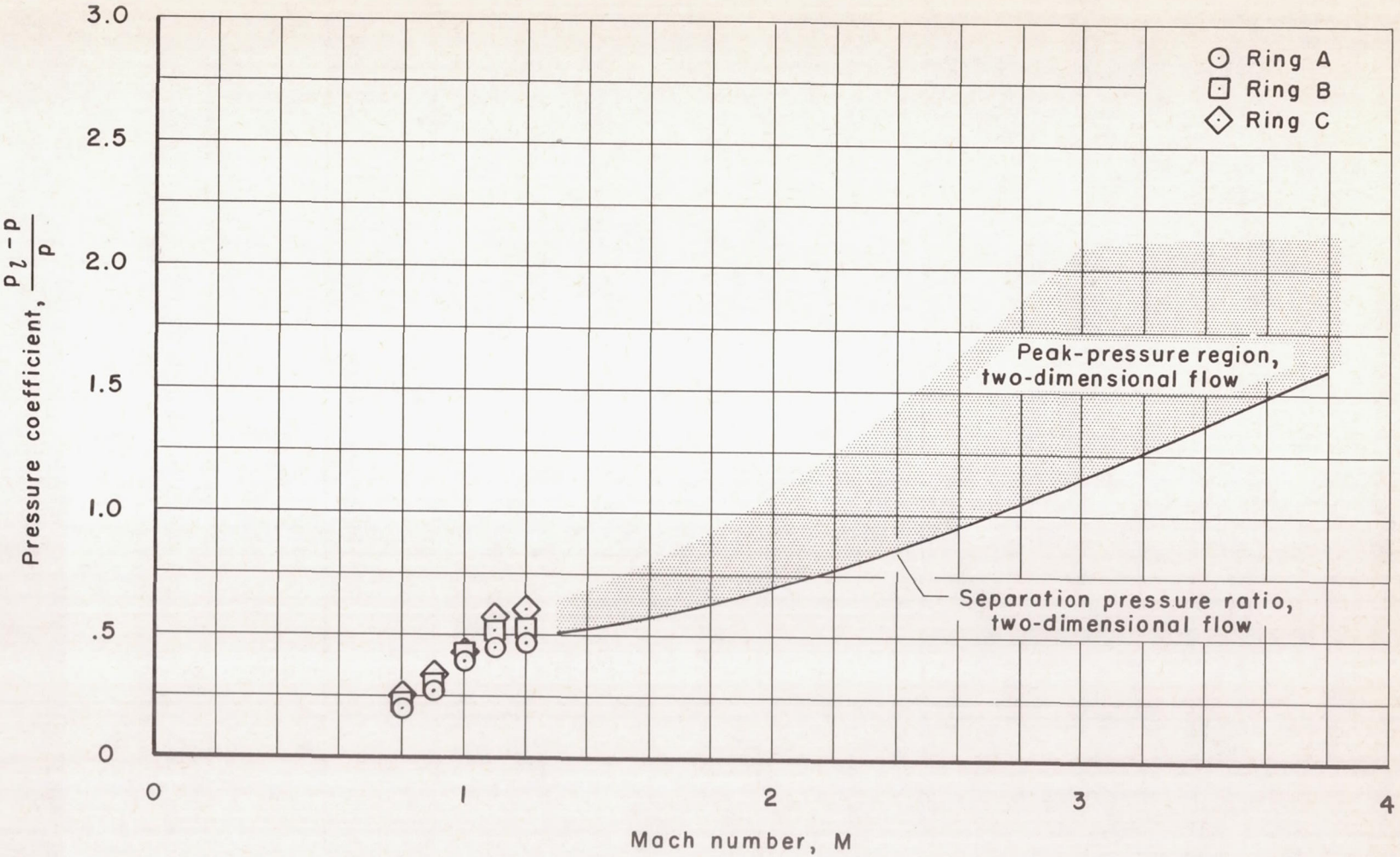

Figure 15.- Peak-pressure coefficients on the body surface ahead of the forward-facing steps compared with two-dimensional data from reference 7.

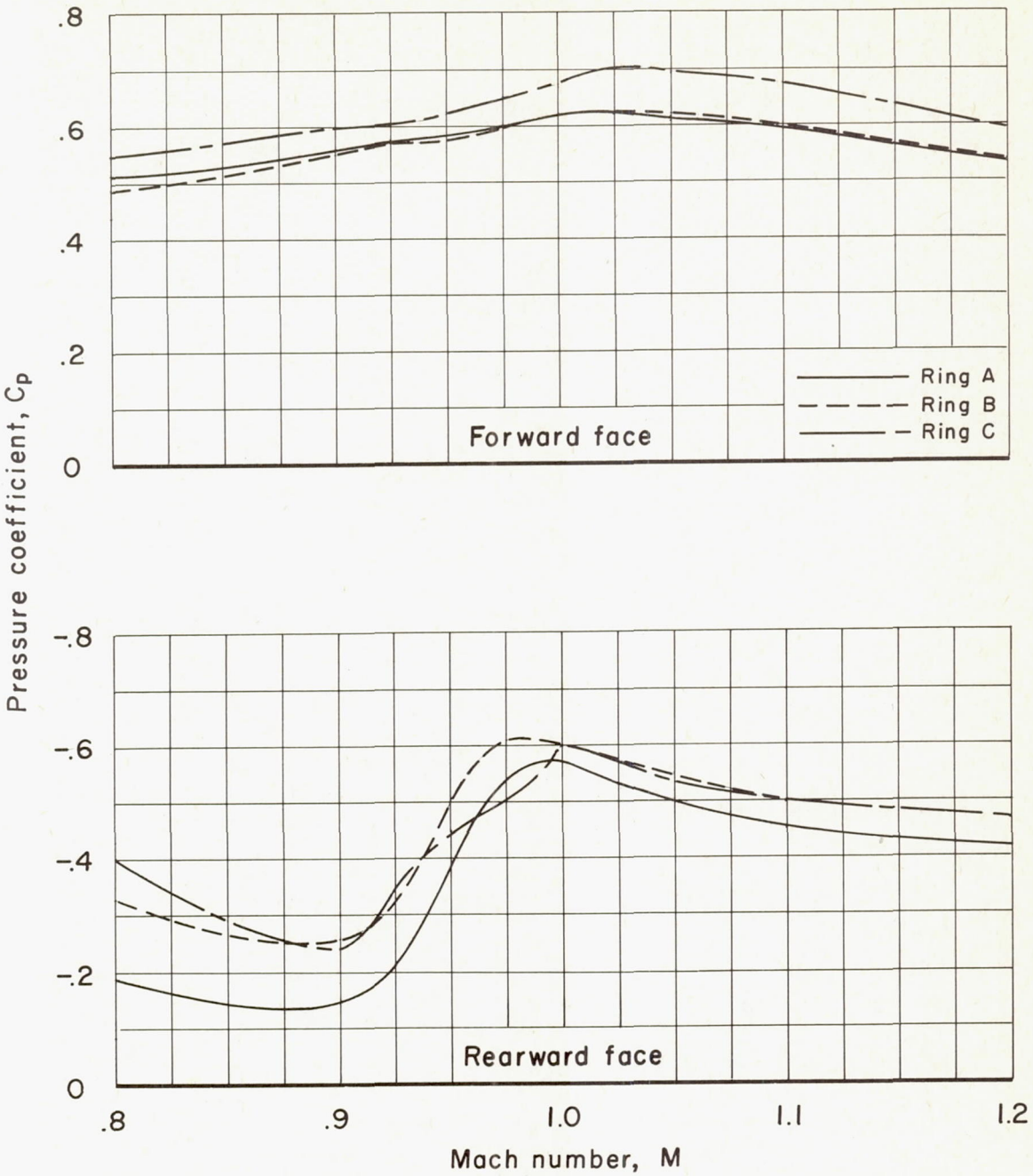

Figure 16.- Pressure coefficients obtained from orifices on the forward and rearward faces of ring A and from the body orifice locations closest to the faces of rings B and C.

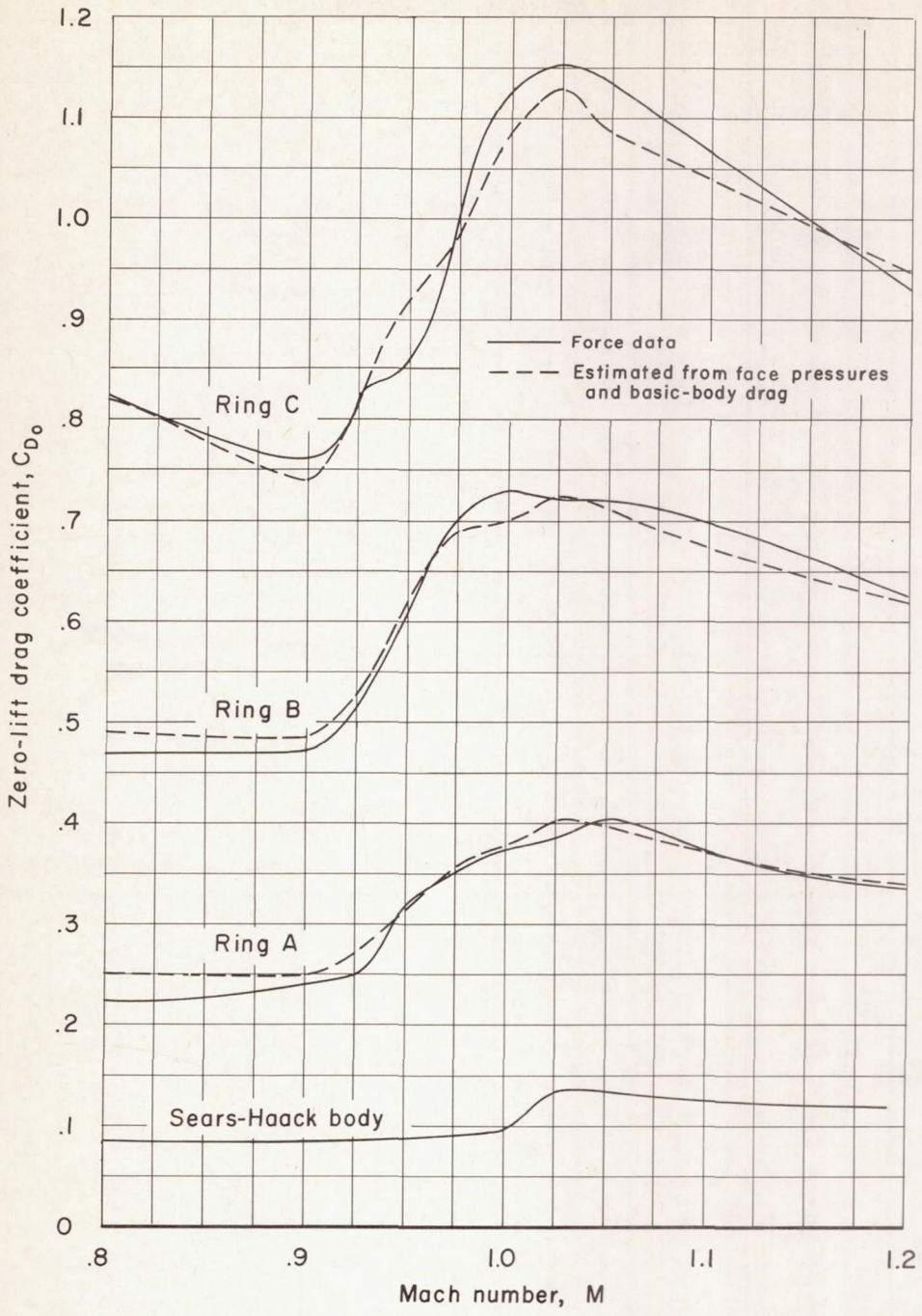

Figure 17.- Zero-lift drag coefficients as determined from the experimental force data and estimated by combining the drag of the Sears-Haack body with the pressure drag based on the pressures acting on the faces of the rings.

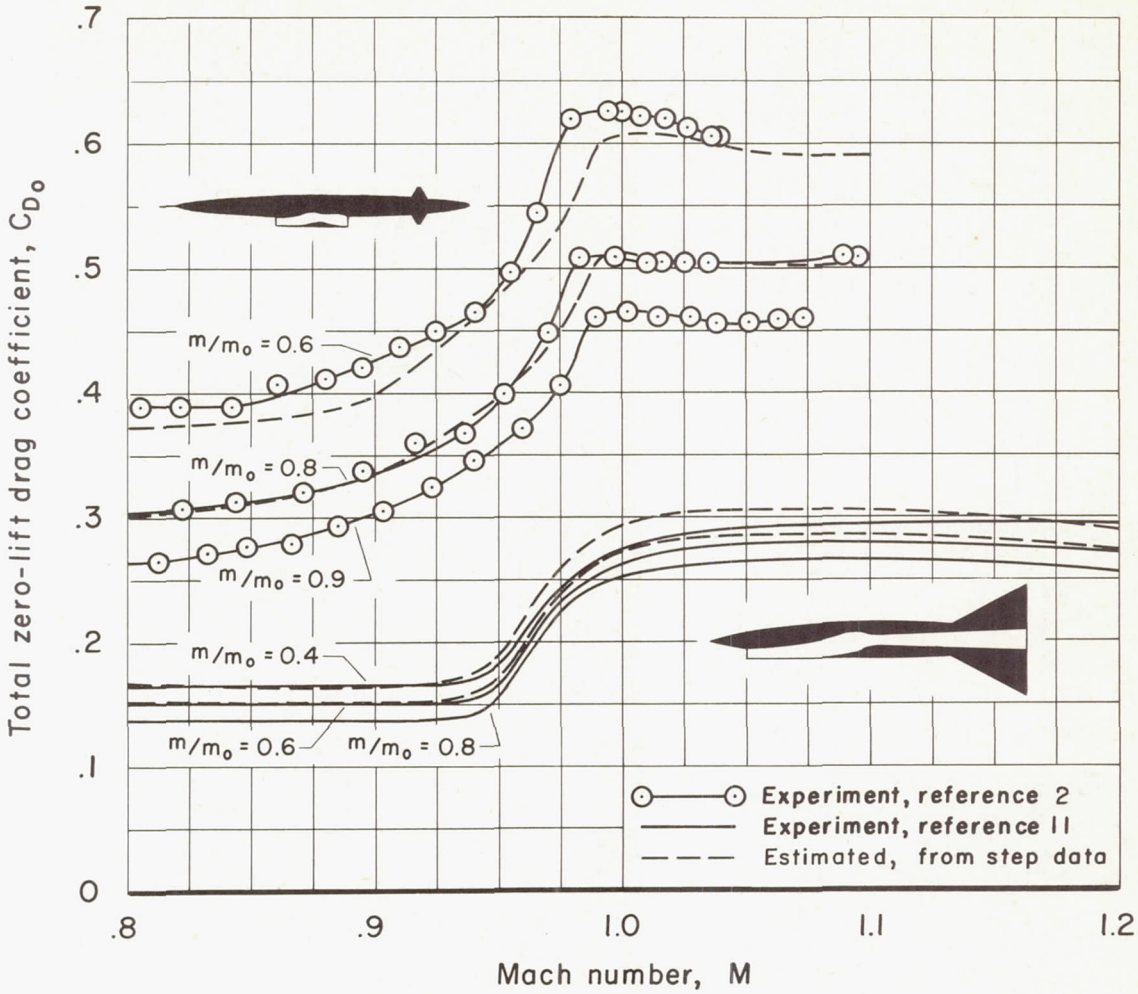

Figure 18.- Effect of reduced mass-flow ratio on the total drag coefficients of two different duct models with drag increases estimated from experimental pressures on the faces of ring A.